ตัวกลางยืดหยุ่นหลายชั้นภายใต้แรงกระทำสมมาตรตามแนวแกนและผลกระทบจากพลังงานที่ผิว

นายคณิน ฐานถิร

วิทยานิพนธ์นี้เป็นส่วนหนึ่งของการศึกษาตามหลักสูตรปริญญาวิศวกรรมศาสตรมหาบัณฑิต
สาขาวิชาวิศวกรรมโยธา ภาควิชาวิศวกรรมโยธา
คณะวิศวกรรมศาสตร์ จุฬาลงกรณ์มหาวิทยาลัย
ปีการศึกษา 2560

MULTI-LAYERED ELASTIC MEDIUM UNDER AXISYMMETRIC LOADING AND SURFACE ENERGY EFFECTS

Mr. Kanin Tarntira

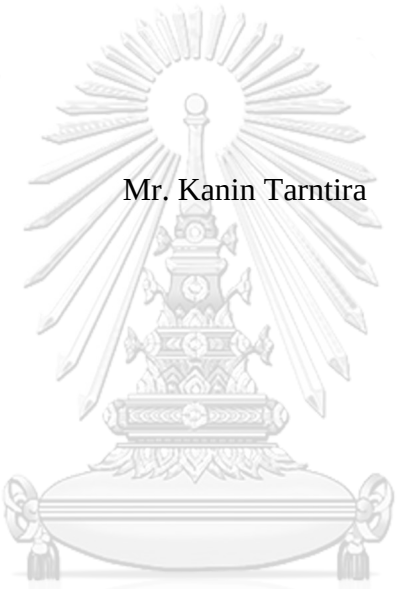

A Thesis Submitted in Partial Fulfillment of the Requirements
for the Degree of Master of Engineering Program in Civil Engineering
Department of Civil Engineering
Faculty of Engineering
Chulalongkorn University
Academic Year 2017

Thesis Title	MULTI-LAYERED ELASTIC MEDIUM UNDER AXISYMMETRIC LOADING AND SURFACE ENERGY EFFECTS
By	Mr. Kanin Tarntira
Field of Study	Civil Engineering
Thesis Advisor	Professor Teerapong Senjuntichai, Ph.D.

Accepted by the Faculty of Engineering, Chulalongkorn University in Partial Fulfillment of the Requirements for the Master's Degree

.....Dean of the Faculty of Engineering
(Associate Professor Supot Teachavorasinskun, D.Eng.)

THESIS COMMITTEE

.....Chairman
(Associate Professor Jaroon Rungamornrat, Ph.D.)

.....Thesis Advisor
(Professor Teerapong Senjuntichai, Ph.D.)

.....External Examiner
(Wichairat Kaewjuea, Ph.D.)

คณิน ฐานถิร : ตัวกลางยืดหยุ่นหลายชั้นภายใต้แรงกระทำสมมาตรตามแนวแกนและผลกระทบจากพลังงานที่ผิว (MULTI-LAYERED ELASTIC MEDIUM UNDER AXISYMMETRIC LOADING AND SURFACE ENERGY EFFECTS) อ.ที่ปรึกษาวิทยานิพนธ์หลัก: ศ. ดร. ธีรพงศ์ เสนจันทร์ตีไชย, 46 หน้า.

ในทุกวันนี้โครงสร้างหลายชั้นระดับนาโนได้ถูกใช้งานหลากหลายรูปแบบ เนื่องจากผลกระทบจากพลังงานที่ผิวมีความสำคัญที่ระดับนาโน รูปแบบวิธีการคำนวณที่พิจารณาผลกระทบนี้จึงมีความจำเป็นในการวิเคราะห์พฤติกรรมทางกลของโครงสร้างเหล่านั้นได้อย่างแม่นยำ งานวิจัยชิ้นนี้ นำเสนอระเบียบวิธีการแก้ปัญหาเพื่อใช้ในการวิเคราะห์โครงสร้างยืดหยุ่นหลายชั้นภายใต้ผลกระทบจากพลังงานที่ผิวและแรงกระทำสมมาตร โดยใช้ทฤษฎีของเกอร์ตินและเมอร์ดอค ฟังก์ชันมาตรฐานของเลิฟและวิธีการแปลงแฮงเคลได้ถูกนำมาใช้เพื่อพัฒนาคำตอบทั่วไป และสร้างเมทริกซ์ความสัมพันธ์ขึ้นมาในแต่ละชั้น เมทริกซ์ความสัมพันธ์ของระบบโครงสร้างหลายชั้นได้ถูกประกอบขึ้นโดยคำนึงถึงความต่อเนื่องของแรงและการกระจัดจากแต่ละผิวระหว่างชั้น ผลลัพธ์เชิงตัวเลขที่ได้จากการแก้ปัญหาสมการระบบโครงสร้างเป็นผลลัพธ์ของการกระจัดและความเค้นของแต่ละผิวระหว่างชั้นตัวกลางภายใต้แรงกระทำสมมาตร ผลที่ได้รับแสดงให้เห็นว่าการกระจัดและความเค้นได้รับผลกระทบจากคุณสมบัติที่ผิว รัศมีของแรงกระทำ และคุณสมบัติของวัสดุในแต่ละชั้น รูปแบบวิธีการแก้ปัญหาที่ได้เสนอไปนั้นสามารถนำไปใช้ในการศึกษาปัญหาที่อาจจะพบในงานที่เกี่ยวข้องกับนาโนเทคโนโลยี และผลการศึกษาที่ได้รับยังสามารถใช้เป็นพื้นฐานในการพัฒนาการแก้ระเบียบวิธีเชิงตัวเลข เช่น วิธีการทางไฟไนต์เอลิเมนต์ และ วิธีการทางบาวดารี่เอลิเมนต์ สำหรับการแก้ปัญหาระบบโครงสร้างหลายชั้นที่ได้คำนึงถึงผลของพลังงานที่ผิว ที่มีความซับซ้อนมากยิ่งขึ้น

ภาควิชา วิศวกรรมโยธา ลายมือชื่อนิสิต .....

สาขาวิชา วิศวกรรมโยธา ลายมือชื่อ อ.ที่ปรึกษาหลัก .....

ปีการศึกษา 2560

5970116921 : MAJOR CIVIL ENGINEERING
KEYWORDS: GURTIN-MURDOCH MODEL / MULTI-LAYERED MEDIUM / SURFACE ENERGY EFFECTS

KANIN TARNTIRA: MULTI-LAYERED ELASTIC MEDIUM UNDER AXISYMMETRIC LOADING AND SURFACE ENERGY EFFECTS. ADVISOR: PROF. TEERAPONG SENJUNTICHAI, Ph.D., 46 pp.

Multi-layered nano-scale structures have been found in a wide range of applications these days. Since the surface energy effect is presented at the nano-scale level, a novel calculation scheme is required to accurately capture the mechanical behaviors of such structures. In this study, a solution scheme for analysis of a multi-layered elastic medium with influence of surface energy effects subjected to axisymmetric loading by adopting Gurtin-Murdoch surface elasticity theory is presented. The standard Love's representation and Hankel integral transform are employed to derive the general solutions, and the obtained solutions are employed in the determination of the stiffness matrix for each elastic layer. The global stiffness equation of a multi-layered system is assembled by considering the continuity of traction and displacements at each layer interface. The numerical solutions to the global equation yield displacements and stresses at the interfaces of the layered medium under axisymmetric loading. The obtained results reveal that the elastic fields are significantly influenced by the surface elastic properties, the loading radius and the elastic material properties of each layer. The proposed solution scheme can be used to examine a variety of practical problems, and the solutions can also be used as benchmark solutions in the development of FEM and BEM for more complicated problems related to multi-layered systems with the influence of surface energy effects.

Department:	Civil Engineering	Student's Signature	.....
Field of Study:	Civil Engineering	Advisor's Signature	.....
Academic Year:	2017		

ACKNOWLEDGEMENTS

This study was supported by the Civil Engineering 100-year Chula scholarship. This support is thankfully acknowledged.

First, I wish to express my sincere appreciation to my thesis advisor, Professor Dr. Teerapong Senjuntichai, for his supports on my work. His priceless advices and great encouragements help me to go through every works throughout the course in Chulalongkorn University. Moreover, I do appreciate countless of valuable suggestions from my senior colleagues, Mr. Supakorn Tirapat and Mr. Suraparb Keawsawasvong, which help me go through hard times, owe my loving thanks to my family for supporting me unconditionally. Finally, I would like to thank everyone who has supported directly and indirectly in every processes of the study, this thesis would not be successful without everyone.

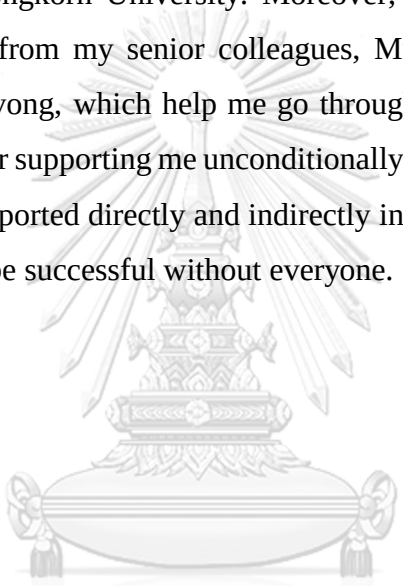

CONTENTS

LIST OF TABLES

LIST OF FIGURES

Figure Page

LIST OF ABBREVIATIONS

a	loading radius;
$\mathbf{c}(\bar{\xi})$	matrix contained Hankel arbitrary functions of each layer;
$\mathbf{F}^*$	vector of external force at the n^{th} surface;
h	thickness of an elastic layer;
H	total thickness of the whole medium;
$H(a-r)$	Heaviside step function;
$J_n(\xi)$	Bessel functions of the first kind of order n;
$\mathbf{K}^{(n)}$	stiffness matrix of the n^{th} layer;
$\mathbf{K}^*$	global stiffness matrix of the medium;
$\bar{m}$	grading parameter;
n	layer or surface index;
n_i	unit normal vector in the i-direction;
N	number of layers;
$p(r)$	an applied normal traction;
p_o	magnitude of loads;
$q(r)$	an applied tangential traction;
r	radial coordinate;
$\mathbf{R}(\bar{\xi},\bar{z})$	displacement matrix of the bulk material;
$\mathbf{S}(\bar{\xi},\bar{z})$	stress matrix of the bulk material;
t_i^0	surface traction in the i-direction;
T_α^s	surface stress term in the i-direction;
u_i	displacement of the bulk material in the i-direction;
u_α^s	displacement of the surface in the α-direction;
$\mathbf{U}^*$	generalized displacement vector of the equation system;
$\mathbf{u}^{(n)}$	displacement vector for the n^{th} layer;
z	vertical coordinate;

$\mathbf{Z}_n(\bar{\xi},\bar{z})$	surface stress matrix of the n^{th} surface;
γ_n	radial-direction nondimensional surface parameter;
δ_n	vertical-direction nondimensional surface parameter;
δ_{ij}	Kronecker delta;
ε_{ij}	strain components of the bulk material;
$\varepsilon^s_{\beta\alpha}$	surface strain components of the surface;
κ^s	surface material constant;
λ	Lame' constant of the bulk material;
λ^s	surface Lame' constant of the material;
Λ	material length scale;
μ	Lame' constant of the bulk material;
μ^s	surface Lame' constant of the material;
ξ	integral transform parameter;
σ_{ij}	stress components of the bulk material;
$\sigma^s_{\beta\alpha}$	surface stress components of the surface;
$\boldsymbol{\sigma}^{(n)}$	stress vector for the n^{th} layer;
τ^s	residual surface stress;
τ_R	ratio of the interface residual surface stress to the top surface's;
Φ	Love's strain potential;
ω	sum of the Lame's constant and the shear modulus;
∇^2	Laplacian operator

CHAPTER I

INTRODUCTION

1.1 GENERAL

One of the most important research areas that have gained a lot of attentions during the past two these decades is nano-mechanics. There is a significant growth in the applications related to the nano-scale structures recently such as electronic conductors, magnetic storage mediums and hard surface coatings. Some highlights of utilizing nano-scale structures are the size of the structures, which have at least one of the overall dimensions is between 1 and 100 nano-meter [1], and some special properties or behaviors that become significant when the structure size is reduced to nano-scale such as size-dependent behavior [2]. Despite those benefits, another effect, which is usually ignored at the macro-scale structure, has to be considered in the set of governing equations of the nano-structure system called the surface free energy effects. Various models have been formulated to capture the size-dependent behavior but the model established by Gurtin and Murdoch [3, 4], called the theory of surface elasticity, is selected in this study due to its attractive features both in terms of computational efficiency and level of accuracy gained. The model is later proven promising by atomistic and molecular static simulations of nano-scale plates and bars subjected to uniaxial loading and pure bending conducted by Miller and Shenoy, [5]. The Gurtin-Murdoch model has been utilized by many researchers to solve various solid mechanics problems in which all the studies were also taken into account the surface energy effects. Such problems can be simply classified as the problems of an elastic layer, with either an underlying rigid base or half-space, undergoing axisymmetric or plane-strain deformations. Despite many problems with the surface energy effects being widely examined in recent decades, a multi-layered structure is one of the structure types that has not been extensively investigated when the surface stress influence is considered.

Multi-layered structures have been used for centuries in many interesting problems in the fields such as aerospace engineering, electrical engineering, geomechanics etc. The concept of multi-layered structure is that the structure is

constructed with a number of layers in which material properties and thickness of each layer can be different. Being able to possess multiple properties makes multi-layered structure system more suitable to many practical situations than the conventional homogeneous structural system. While mechanical behavior of the multi-layered structures has been vastly studied for many decades, none of them takes into account the surface energy effects. This study presents a novel solution scheme for an analysis of a multi-layered elastic medium subjected to axisymmetric loading with the surface energy effects by adopting the Gurtin-Murdoch surface elasticity theory. After the scheme is fully developed, several parameters of the multi-layered structures are then studied to understand their influences on mechanical behaviors. The solutions obtained from this study can also be used as benchmarks solutions in the development of various analytical approaches, such as FEM and BEM, and provide the useful mechanical behaviors of the multi-layered structures when the surface energy effects are considered.

1.2 OBJECTIVES AND SCOPES OF THE PRESENT STUDY

The objectives and scopes of this study are:

1. To develop an efficient solution scheme for investigating a multi-layered elastic medium under axisymmetric loading and surface energy effects.

2. To investigate the influence from various parameters, such as material parameters, surface properties, layering, size dependency etc., on elastic fields of a multi-layered elastic medium under axisymmetric loading and surface energy effects.

CHAPTER II

LITERATURE REVIEWS

For more than a century, the effect of surface was noticed and introduced by Gibbs [6]. The definition of surface quantities was defined, which is the surface free energy as the reversible work per unit area needed to create a new surface and, for the solid surface, the surface stress as the reversible work per unit area needed to elastically stretch a pre-existing surface. Therefore, the correlation between the surface free energy and the surface stress was developed from the thermodynamics of solid surfaces which refer the surface stress as a term of variation of the surface free energy with respect to the surface strain [7]. In addition, another important quantity used to illustrate the influence of surface energy effect is the ratio of surface free energy and Young's modulus, which is a parameter with a dimension of length [8]. The value of this length, called the intrinsic length, in the case of a soft solid, is much higher than a conventional solid due to the smaller number of their elastic modulus and thus the surface influence becomes significant [9]. Apart from these discoveries, the surface elasticity is still the attractive fields to be explored by many researchers, especially in the area of mechanics of surface.

Plenty of approaches have been used by many scientists to capture the mechanical behaviors of nano-scale structures, which exhibits the noticeable surface energy influence due to its dimension. In this study, the continuum mechanics approach is chosen due to its attractive features in terms of computational efficiency and level of accuracy gained. To study the mechanical behavior at nano-scale level in the context of continuum mechanics, a mathematical framework known as the theory of surface elasticity, which is based on the modified continuum mechanics concept developed by Gurtin and Murdoch [3, 4], has been employed by many researchers. According to this model, the surface is represented by a zero-thickness layer perfectly bonded to the bulk and is governed by a constitutive law that is different from the bulk material. This surface elasticity model is later proven to be promising and attractive by the supportive results obtained from atomistic and molecular static simulations [5, 10] for modeling a

various kind of nano-scale problems with the consideration of surface energy effects. Furthermore, despite the surface stresses are generally anisotropic and surface crystallographic direction dependent [10], but in the analysis of nano-scale problems, it is acceptable and sufficient to consider the stresses as isotropic due to the effort used to compute anisotropic surface stresses is prohibitive. Another well-known continuum based theory which developed to take into account the size-dependent material behavior is the strain gradient elasticity theory by Mindlin [11]. Even the theory has not been extensively employed due to the higher-order governing equations, its simplified version was then developed to obtain the analytical solution of numerous continuum mechanics problems [12].

Analytical solutions of many problems in the context of continuum mechanics have been widely examined by adopting the Gurtin-Murdoch model to study various kinds of boundary value problems with the consideration of surface energy influence over last several decades. For instance, several researchers investigated the problems involving nano-inclusions and nano-inhomogeneities [13], ultra-thin elastic film [14], thin plate [15], nano-indentation problems [16], elastic layer on rigid foundation [17, 18], crack problems [19, 20], nanoplates [21] and elastic layer on half-space [22].

Despite the surface influence on many problems has been extensively studied by using the continuum mechanics, stress analysis of a multi-layered structure has not been reported in the literature when the surface influence is considered. To emphasize the significance of multi-layered structures, a great number of problems can be found such as most electrical circuits in electrical engineering, composite laminate materials which used in aerospace engineering and construction [23], micro- and nano-electro-mechanical system (MEMS and NEMS). Extensive studies have been conducted to examine this type of structures in many applications without the surface energy effects, for instance, T. Senjuntichai, R.K.N.D. Rajapakse and Y. Sapsathiarn studied mechanics of multi-layered poroelastic medium in terms of statics and dynamics subjected to axisymmetric and plane conditions [24-26], the dispersion of shear and surface waves in multi-layered solid media are investigated by Haskell [27], Zhu et al. [28] used X-ray diffraction, transmission electron microscopy and nanoindentation to investigate the microstructure, hardness and creep behavior of Cu/Ni multi-layered structure where the thickness of layers are in nanoscale. Focusing on nano-scale

structures, a multi-layered nano structures can be seen in a wide range of nano-scale inventions such as semiconductor materials, dielectric, insulating materials, magnetic/optical storage mediums and hard surface coatings [28, 29]. However, the presence of the surface energy effects makes nano-scale mechanics of the multi-layered structures different from those in macro-scale. In this study, a numerical solution scheme based on continuum mechanic is constructed with the capability to analyze multi-layered structures when the surface energy effect is included. By treating the medium as an elastic continuum, the results from the continuum scheme can be obtained with relatively low usage of computational resources compared to those obtained by atomistic simulations. Although the results from the continuum model is approximated but the accuracy level is still acceptable and high enough to make the model quite attractive to researchers. Moreover, the combination of the multi-layered solution scheme and the influence of the surface energy effects presented in this study allows users to examine several problems of multi-layered structures with the surface effects being considered. Thus, this research is essential to provide important information on mechanical behaviors of this particular multi-layered structures to other researchers for further studies in the area of nano-mechanics.

CHAPTER III

EXACT STIFFNESS MATRIX SCHEME

This chapter starts with the basic equations and general solutions that can be applied to solve the boundary value problems of a multi-layered elastic medium, with the surface energy effects, resting on a rigid base as shown in Figure 3.1. The basic governing equations of bulk and surface materials with the consideration of surface effects based on Gurtin-Murdoch model are expressed. The standard Love's representation and Hankel integral transform are employed to derive the general solutions of the bulk material. Thereafter, an exact stiffness matrix scheme, which is used to solve the boundary value problem, is presented. The stiffness matrices for each layer can be obtained from the general solutions for displacements and stresses expressed in the Hankel transform space. The global stiffness matrix is obtained by considering the boundary and continuity of traction and displacements at the boundary and interfaces. The solution to the global equation system yields the displacements and stresses in the Hankel transform space at the top surface and each interface of the multi-layered elastic medium under surface energy effects and axisymmetric loading.

3.1 BASIC EQUATIONS

Consider an elastic medium under the influence of surface energy at surface subjected to the applied traction on its surface. According to Gurtin-Murdoch surface elasticity theory, the medium consists of two different parts, i.e. the bulk material and the surface, which is a zero-thickness layer perfectly bonded to the bulk material without slipping. The field equations of the bulk material are identical to those given by the classical elasticity. For the surface, the field equations are represented by the generalized Young-Laplace equation [30]. The material constants of the bulk are also different to those at the surface.

The governing equations of bulk material, which are the equilibrium equation, constitutive law and kinematics relationship, without the body forces are shown below respectively:

$$\sigma_{ij,j}=0 \tag{3.1a}$$

$$\sigma_{ij}=2\mu\varepsilon_{ij}+\lambda\delta_{ij}\varepsilon_{kk} \tag{3.1b}$$

$$\varepsilon_{ij}=\frac{1}{2}\left(u_{i,j}+u_{j,i}\right) \tag{3.1c}$$

where the terms σ_{ij}, ε_{ij} and u_i represent the stress tensor components, strain tensor components and displacement vector components respectively. In addition, Lamé constants of bulk material are denoted by λ and μ.

The governing equations of the surface, expressed by the generalized Young-Laplace equation [3, 4, 30], are given for boundary conditions for surface element, surface constitutive law and surface kinematics relationship respectively as

$$\sigma^s_{i\alpha,\alpha}+\sigma_{ij}n_j+t^0_i=0 \tag{3.2a}$$

$$\sigma^s_{\beta\alpha}=\tau^s\delta_{\beta\alpha}+2\left(\mu^s-\tau^s\right)\varepsilon_{\beta\alpha}+\left(\lambda^s+\tau^s\right)\varepsilon_{\gamma\gamma}\delta_{\beta\alpha}+\tau^s u^s_{\beta,\alpha};\sigma^s_{3\alpha}=\tau^s u^s_{3,\alpha} \tag{3.2b}$$

$$\varepsilon^s_{\alpha\beta}=\frac{1}{2}\left(u^s_{\alpha,\beta}+u^s_{\beta,\alpha}\right) \tag{3.2c}$$

In eq. (3.2), the surface quantity terms are labeled by the superscript "s". The material constants λ^s, μ^s and τ^s represent the surface Lamé constants of the surface and the residual surface stress or surface tension under unstrained condition respectively; n_j denotes the unit normal vector to the surface; and t^0_i denotes the prescribed surface traction. It should be noted that, for a given surface orientation of a pure/semiconductor at a specific temperature, the value of τ^s is constant. In addition, the Greek subscripts, α, β and γ, denote the field quantities of the

surface and employ the value of 1 and 2, while the Latin subscripts, i, j and k, take the value of 1, 2 and 3.

The third term in eq. (3.2b) is the out-of-plane component of the surface stress that is the pre-existing surface tension in the deformed configuration multiplied with the out-of-plane surface gradient which its unit vector tangent to the surface in the deformed state. This term is often ignored in past studies that employed the Gurtin-Murdoch theory as results of the assumption of infinitesimal deformations in undeformed configuration. In contrast, the contribution to the constitutive equation, eq. (3.2b), of the out-of-plane term is not negligible in the deformed state and of the same order as other terms. Thus, even in the case of small deformations, this out-of-plane term could become significant [16, 18, 20, 31]. The governing equations for the bulk material and the surface for the case of axisymmetric problems are presented next.

3.2 GENERAL SOLUTIONS FOR AXISYMMETRIC PROBLEMS

Consider a cylindrical coordinate system (r, θ, z), which is rotationally symmetric about the z-axis. The field equations of the bulk material undergoing axisymmetric deformations are identical to the classical governing equations [32]. On the surface, the field equations can be expressed as generalized Young-Laplace equations [30], surface constitutive relations and strain-displacement relations [3, 4]. The generalized Young-Laplace equations of the surface are given by

$$\frac{d\sigma_{rr}^{s}}{dr}+\frac{\sigma_{rr}^{s}-\sigma_{\theta\theta}^{s}}{r}+\sigma_{zr}\big|_{z=0}+t_{r}^{0}=0 \tag{3.3a}$$

$$\frac{d\sigma_{zr}^{s}}{dr}+\frac{\sigma_{zr}^{s}}{r}+\sigma_{zz}\big|_{z=0}+t_{z}^{0}=0 \tag{3.3b}$$

The surface constitutive relations are

$$\sigma_{rr}^{s}=\tau^{s}+\left(\lambda^{s}+2\mu^{s}\right)\varepsilon_{rr}^{s}+\left(\lambda^{s}+\tau^{s}\right)\varepsilon_{\theta\theta}^{s} \tag{3.3c}$$

$$\sigma_{\theta\theta}^{s} = \tau^{s} + \left(\lambda^{s} + 2\mu^{s}\right)\varepsilon_{\theta\theta}^{s} + \left(\lambda^{s} + \tau^{s}\right)\varepsilon_{rr}^{s} \tag{3.3d}$$

$$\sigma_{zr}^{s} = \tau^{s}\frac{du_{z}^{s}}{dr} \tag{3.3e}$$

In addition, the strain-displacement relations of the surface are

$$\varepsilon_{rr}^{s} = \frac{du_{r}^{s}}{dr} \tag{3.3f}$$

$$\varepsilon_{\theta\theta}^{s} = \frac{u_{r}^{s}}{r} \tag{3.3g}$$

where t_r^0 and t_z^0 denote the traction applied on radial and vertical directions respectively.

For axisymmetric problems, the governing equation of the bulk material is expressed in the following biharmonic equation [32].

$$\nabla^2\nabla^2\Phi = 0 \tag{3.4}$$

where Φ is Love's strain potential and ∇^2 represents the Laplacian operator in the cylindrical coordinate, which can be expressed as,

$$\nabla^2 = \frac{\partial^2}{\partial r^2} + \frac{1}{r}\frac{\partial}{\partial r} + \frac{\partial^2}{\partial z^2} \tag{3.5}$$

Applying the Hankel integral transform to eq. (3.4) results in

$$\int_0^\infty r\nabla^2\nabla^2\Phi J_0\left(\xi r\right)dr = \left(\frac{d^2}{dz^2} - \xi^2\right)^2 \Phi\left(\xi, z\right) = 0 \tag{3.6}$$

where

$$\Phi(\xi,z)=\int_0^\infty \Phi J_0(\xi r)\,r dr \tag{3.7}$$

and $J_n(\xi)$ denotes the Bessel functions of the first kind of order n. The solution to the eq. (3.6) is given by

$$\Phi(\xi,z)=(A+Bz)e^{-\xi z}+(C+Dz)e^{\xi z} \tag{3.8}$$

where A, B, C and D are the arbitrary functions to be obtained by applying the appropriate boundary conditions.

Consequently, the general solutions for stresses and displacements in the bulk material can be expressed, in a cylindrical coordinate, as shown below [32]:

$$\sigma_{rr}=\int_0^\infty \xi\left[\lambda\frac{d^3\Phi}{dz^3}+(\lambda+2\mu)\xi^2\frac{d\Phi}{dz}\right]J_0(\xi r)\,d\xi-\frac{2(\lambda+\mu)}{r}\int_0^\infty \xi^2\frac{d\Phi}{dz}J_1(\xi r)\,d\xi \tag{3.9a}$$

$$\sigma_{\theta\theta}=\lambda\int_0^\infty \xi\left[\frac{d^3\Phi}{dz^3}-\xi^2\frac{d\Phi}{dz}\right]J_0(\xi r)\,d\xi+\frac{2(\lambda+\mu)}{r}\int_0^\infty \xi^2\frac{d\Phi}{dz}J_1(\xi r)\,d\xi \tag{3.9b}$$

$$\sigma_{zz}=\int_0^\infty \xi\left[(\lambda+2\mu)\frac{d^3\Phi}{dz^3}-(3\lambda+4\mu)\xi^2\frac{d\Phi}{dz}\right]J_0(\xi r)\,d\xi \tag{3.9c}$$

$$\sigma_{zr}=\int_0^\infty \xi^2\left[\lambda\frac{d^2\Phi}{dz^2}+(\lambda+2\mu)\xi^2\Phi\right]J_1(\xi r)\,d\xi \tag{3.9d}$$

$$u_r=\frac{\lambda+\mu}{\mu}\int_0^\infty \xi^2\frac{d\Phi}{dz}J_1(\xi r)\,d\xi \tag{3.9e}$$

$$u_z=\int_0^\infty \xi\left[\frac{d^2\Phi}{dz^2}-\frac{\lambda+2\mu}{\mu}\xi^2\Phi\right]J_0(\xi r)\,d\xi \tag{3.9f}$$

3.3 BOUNDARY VALUE PROBLEM

The boundary value problem of a multi-layered elastic medium under surface stress influence and axisymmetric surface loading is presented in this section. The layers and the surfaces of the multi-layered medium is shown in Figure 3.1 where the 2nd to the N^{th} surface could be called “interface”. The stress

boundary conditions at the top surface and the displacement boundary conditions at the rigid base of the multi-layered medium as shown in Figure 3.1 are given below.

$$-\left\{\sigma_{zz}^{(1)}+T_z^s\right\}\Big|_{z=z_1}=p(r) \tag{3.10a}$$

$$-\left\{\sigma_{zr}^{(1)}+T_r^s\right\}\Big|_{z=z_1}=q(r) \tag{3.10b}$$

$$u_\alpha\Big|_{z=z_{N+1}}=0 \tag{3.10c}$$

where $\alpha=r,z$ and

$$T_z^s\Big|_{z=z_1}=\left[\frac{d\tau_1^s}{dr}\left(\frac{du_z^s}{dr}\right)_{z=z_1}+\tau_1^s\left(\frac{d^2u_z^s}{dr^2}+\frac{1}{r}\frac{du_z^s}{dr}\right)_{z=z_1}\right] \tag{3.10d}$$

$$T_r^s\Big|_{z=z_1}=\left[\frac{d\tau_1^s}{dr}\left(1+\frac{u_r^s}{r}\right)_{z=z_1}+\kappa_1^s\left(\frac{d^2u_r^s}{dr^2}+\frac{1}{r}\frac{du_r^s}{dr}-\frac{u_r^s}{r^2}\right)_{z=z_1}\right] \tag{3.10e}$$

In addition, $\kappa_1^s=2\mu_1^s+\lambda_1^s$ is a surface material constant corresponding to the 1st material surface properties. The superscript denotes the index of the layer and the subscript stands for the index number of the surface, normally represented by the parameter n which takes the value of 1 to N for the layer index and $N+1$ for the surface index. Apart from those indices, the superscript letter "s" is shown to denote the surface parameters. The terms $p(r)$ and $q(r)$ are the axisymmetric traction, applying in the normal and tangential directions respectively, on the top surface. The terms u_z^s and u_r^s are the displacements of the surface corresponding to their subscript which have the displacements continuity condition which means each surface is adhered to the nearby lower boundary of the upper layer and the upper boundary of the lower layer without slipping. In addition, the terms T_z^s and T_r^s represent the contribution from the surface energy effects in the normal and tangential directions respectively. These terms are normally ignored in the macro-

scale problems but in the nano-scale problems, these effects have to be considered at the top surface and every interface. Thus, the traction and displacements continuity conditions at the n^{th} surface, where $n = 2,3,...,N$, can be written as the following equations.

$$\left\{\sigma_{zz}^{(n-1)} - \sigma_{zz}^{(n)} - T_z^s\right\}\Big|_{z=z_n} = 0 \tag{3.11a}$$

$$\left\{\sigma_{zr}^{(n-1)} - \sigma_{zr}^{(n)} - T_r^s\right\}\Big|_{z=z_n} = 0 \tag{3.11b}$$

$$u_\alpha^{(n)}\Big|_{z=z_n} = u_\alpha^s\Big|_{z=z_n} = u_\alpha^{(n-1)}\Big|_{z=z_n} \tag{3.11c}$$

The terms on the right-hand side of the eqs. (3.11a) and (3.11b) can be referred to the discontinuity of traction at the n^{th} surface. Since the present problem is subjected to only the top surface loading, the terms on the right-hand side are equal to zero. However, if there is traction applied at the layer interface, the right-hand side terms are non-zero and this calculation scheme is still viable.

To solve this boundary value problem, the continuity condition of traction and displacements at each surface, eqs. (3.11a) to (3.11c), have to be considered with the boundary conditions, eqs. (3.10a) to (3.10c). For the problem shown in Figure 3.1, the condition number of the equation system is extremely large when using the high value of ξ for the equation system to be solved conventionally due to the presence of mis-matching exponential terms in the equations system [24]. The large condition number indicates the ill-conditioning of the system, which results in the low numerical stability of the system. To avoid the low numerical stability, the exact stiffness matrix scheme, [24, 33], is adopted to solve this boundary value problem related to a multi-layered medium with surface energy effects.

3.4 FORMULATION OF EXACT STIFFNESS MATRIX SCHEME

An exact stiffness matrix method is selected to examine the behaviors of a multi-layered elastic medium from the relationship between the displacements and the stresses at each layer. A multi-layered medium consisting of N layers of

different properties and thicknesses over a rigid base is considered as shown in Figure 3.1. The general solutions given by eqs. (3.9a) to (3.9f), the displacements and the stresses in the bulk, can be expressed in the Hankel transform space in the following matrix form.

$$\left[u_z(\bar{\xi},\bar{z}) \quad u_r(\bar{\xi},\bar{z}) \right]^T = \mathbf{R}(\bar{\xi},\bar{z})\,\mathbf{c}(\bar{\xi}) \tag{3.12a}$$

$$\left[\sigma_{zz}(\bar{\xi},\bar{z}) \quad \sigma_{zr}(\bar{\xi},\bar{z}) \right]^T = \mathbf{S}(\bar{\xi},\bar{z})\mathbf{c}(\bar{\xi}) \tag{3.12b}$$

where

$$\mathbf{c}^{(n)}(\bar{\xi}) = \left[A^{(n)} \quad B^{(n)} \quad C^{(n)} \quad D^{(n)} \right]^T \tag{3.12c}$$

$$\mathbf{R}^{(n)}(\bar{\xi},\bar{z}) = \left(\frac{\omega^{(n)}\bar{\xi}}{\bar{\mu}^{(n)}} \right) \begin{bmatrix} -e^{-\bar{\xi}\bar{z}} & \left(-\bar{z} - \dfrac{2\bar{\mu}^{(n)}}{\omega^{(n)}\bar{\xi}} \right) e^{-\bar{\xi}\bar{z}} & -e^{\bar{\xi}\bar{z}} & \left(-\bar{z} + \dfrac{2\bar{\mu}^{(n)}}{\omega^{(n)}\bar{\xi}} \right) e^{\bar{\xi}\bar{z}} \\ -e^{-\bar{\xi}\bar{z}} & \left(-\bar{z} + \dfrac{1}{\bar{\xi}} \right) e^{-\bar{\xi}\bar{z}} & e^{\bar{\xi}\bar{z}} & \left(\bar{z} + \dfrac{1}{\bar{\xi}} \right) e^{\bar{\xi}\bar{z}} \end{bmatrix} \tag{3.12d}$$

$$\mathbf{S}^{(n)}(\bar{\xi},\bar{z}) = \left(\omega^{(n)}\bar{\xi} \right) \begin{bmatrix} e^{-\bar{\xi}\bar{z}} & \left[\bar{z} + \dfrac{\bar{\mu}^{(n)}}{\omega^{(n)}\bar{\xi}} \right] e^{-\bar{\xi}\bar{z}} & -e^{\bar{\xi}\bar{z}} & \left[-\bar{z} + \dfrac{\bar{\mu}^{(n)}}{\omega^{(n)}\bar{\xi}} \right] e^{\bar{\xi}\bar{z}} \\ e^{-\bar{\xi}\bar{z}} & \left[\bar{z} - \dfrac{\bar{\lambda}^{(n)}}{\omega^{(n)}\bar{\xi}} \right] e^{-\bar{\xi}\bar{z}} & e^{\bar{\xi}\bar{z}} & \left[\bar{z} + \dfrac{\bar{\lambda}^{(n)}}{\omega^{(n)}\bar{\xi}} \right] e^{\bar{\xi}\bar{z}} \end{bmatrix} \tag{3.12e}$$

In addition, the dimensionless quantities from the above equations are defined by

$$\kappa_n^s = 2\mu_n^s + \lambda_n^s \tag{3.13a}$$

$$\Lambda = \frac{\kappa_1^s \left(\lambda^{(1)} + 2\mu^{(1)} \right)}{2\mu^{(1)} \left(\lambda^{(1)} + \mu^{(1)} \right)} \tag{3.13b}$$

$$\bar{\mu}^{(n)} = \frac{\mu^{(n)}}{\mu^{(1)}} \tag{3.13c}$$

$$\bar{\lambda}^{(n)} = \frac{\lambda^{(n)}}{\mu^{(1)}} \tag{3.13d}$$

$$\omega^{(n)} = \bar{\lambda}^{(n)} + \bar{\mu}^{(n)} \tag{3.13e}$$

$$\bar{\kappa}_n^s = \frac{\kappa_n^s}{\mu^{(1)}\Lambda} \tag{3.13f}$$

$$\bar{\tau}_n^s = \frac{\tau_n^s}{\mu^{(1)}\Lambda} \tag{3.13g}$$

$$\gamma_n = \frac{\omega^{(n)}\bar{\kappa}_n^s}{2\bar{\mu}^{(n)}} \tag{3.13h}$$

$$\delta_n = \frac{\omega^{(n)}\bar{\tau}_n^s}{2\bar{\mu}^{(n)}} \tag{3.13i}$$

$$\bar{z} = z / \Lambda \tag{3.13j}$$

$$\bar{r} = r / \Lambda \tag{3.13k}$$

$$\bar{\xi} = \xi\Lambda \tag{3.13l}$$

in which the superscript letter "T" represents the transpose of a vector or a matrix. The superposed bar symbol, "$\bar{\ }$", denotes the non-dimensional quantities with respect to the properties of the first layer, eqs. (3.13a) to (3.13l), where the Tilde symbol, "$\tilde{\ }$", denote the non-dimensional quantities in their Hankel transform space.

For the n^{th} layer, the displacement and the stress vectors of top and bottom surfaces of the bulk can be formulated by using eqs. (3.12a) and (3.12b).

$$\begin{Bmatrix} u_z(\bar{\xi},\bar{z}_n) \\ u_r(\bar{\xi},\bar{z}_n) \\ u_z(\bar{\xi},\bar{z}_{n+1}) \\ u_r(\bar{\xi},\bar{z}_{n+1}) \end{Bmatrix} = \begin{bmatrix} \mathbf{R}^{(n)}(\bar{\xi},\bar{z}_n) \\ \cdots\cdots\cdots\cdots \\ \mathbf{R}^{(n)}(\bar{\xi},\bar{z}_{n+1}) \end{bmatrix} \mathbf{c}^{(n)}(\bar{\xi}) \tag{3.14a}$$

$$\begin{Bmatrix} -\sigma_{zz}(\bar{\xi},\bar{z}_n) \\ -\sigma_{zr}(\bar{\xi},\bar{z}_n) \\ \sigma_{zz}(\bar{\xi},\bar{z}_{n+1}) \\ \sigma_{zr}(\bar{\xi},\bar{z}_{n+1}) \end{Bmatrix} = \begin{bmatrix} -\mathbf{S}^{(n)}(\bar{\xi},\bar{z}_n) \\ \cdots\cdots\cdots\cdots \\ \mathbf{S}^{(n)}(\bar{\xi},\bar{z}_{n+1}) \end{bmatrix} \mathbf{c}^{(n)}(\bar{\xi}) \tag{3.14b}$$

Apart from the stresses in the bulk, due to the presence of the surface energy effects, the terms corresponded to the effect T_z^s and T_r^s need to be considered in the same manner as the stresses. By considering the displacements continuity condition, eq. (3.11c), together with the general solutions of normal displacement, radial displacement and their derivatives, eq. (3.9e) and (3.9f), the surface stresses can be represented as shown in the following equation

$$\begin{Bmatrix} -T_z^s(\bar{\xi},\bar{z}_n) \\ -T_r^s(\bar{\xi},\bar{z}_n) \\ 0 \\ 0 \end{Bmatrix} = \begin{bmatrix} -\mathbf{Z}_n(\bar{\xi},\bar{z}_n) \\ \cdots\cdots\cdots\cdots \\ 0 \end{bmatrix} \mathbf{c}^{(n)}(\bar{\xi}) \tag{3.15a}$$

where $T_z^s(\bar{\xi},\bar{z}_n)$ and $T_r^s(\bar{\xi},\bar{z}_n)$ are the Hankel transform of T_z^s and T_r^s, respectively, and the detail of the matrices $\mathbf{Z}_n$ is shown below

$$\mathbf{Z}_n(\bar{\xi},\bar{z}) = \left(\bar{\xi}^2\right) \begin{bmatrix} -\delta_n e^{-\bar{\xi}\bar{z}} & -\left(\bar{z} + \dfrac{2\bar{\mu}^{(n)}}{\omega^{(n)}\bar{\xi}}\right)\delta_n e^{-\bar{\xi}\bar{z}} & -\delta_n e^{\bar{\xi}\bar{z}} & -\left(\bar{z} - \dfrac{2\bar{\mu}^{(n)}}{\omega^{(n)}\bar{\xi}}\right)\delta_n e^{\bar{\xi}\bar{z}} \\ -\gamma_n e^{-\bar{\xi}\bar{z}} & \left(-\bar{z} + \dfrac{1}{\bar{\xi}}\right)\gamma_n e^{-\bar{\xi}\bar{z}} & \gamma_n e^{\bar{\xi}\bar{z}} & \left(\bar{z} + \dfrac{1}{\bar{\xi}}\right)\gamma_n e^{\bar{\xi}\bar{z}} \end{bmatrix} \tag{3.15b}$$

Thereafter, the relationship between the displacements and the stresses at each layer is formulated. The stresses expressed in this relationship are the stresses in the bulk combining with the surface stresses of the surface located between the layers. From the eqs. (3.14b) and (3.15a), the stresses terms can be merged as shown below.

$$\begin{Bmatrix} -\sigma_{zz}(\bar{\xi},\bar{z}_n) \\ -\sigma_{zr}(\bar{\xi},\bar{z}_n) \\ \sigma_{zz}(\bar{\xi},\bar{z}_{n+1}) \\ \sigma_{zr}(\bar{\xi},\bar{z}_{n+1}) \end{Bmatrix} + \begin{Bmatrix} -T^s_z(\bar{\xi},\bar{z}_n) \\ -T^s_r(\bar{\xi},\bar{z}_n) \\ 0 \\ 0 \end{Bmatrix} = \begin{bmatrix} \mathbf{-S}^{(n)}(\bar{\xi},\bar{z}_n) - \mathbf{Z}_n(\bar{\xi},\bar{z}_n) \\ \cdots\cdots\cdots\cdots\cdots\cdots\cdots\cdots \\ \mathbf{S}^{(n)}(\bar{\xi},\bar{z}_{n+1}) \end{bmatrix} \mathbf{c}^{(n)}(\bar{\xi}) \quad (3.16)$$

In view of eq. (3.14a) and eq. (3.16), the following relationships can be established for the n^{th} layer:

$$\boldsymbol{\sigma}^{(n)} = \mathbf{K}^{(n)}\mathbf{u}^{(n)} \quad (3.17a)$$

where

$$\boldsymbol{\sigma}^{(n)} = \begin{Bmatrix} -\left[\sigma_{zz}(\bar{\xi},\bar{z}_n) + T^s_z(\bar{\xi},\bar{z}_n)\right] \\ -\left[\sigma_{zr}(\bar{\xi},\bar{z}_n) + T^s_r(\bar{\xi},\bar{z}_n)\right] \\ \sigma_{zz}(\bar{\xi},\bar{z}_{n+1}) \\ \sigma_{zr}(\bar{\xi},\bar{z}_{n+1}) \end{Bmatrix} \quad (3.17b)$$

$$\mathbf{u}^{(n)} = \begin{Bmatrix} u_z(\bar{\xi},\bar{z}_n) \\ u_r(\bar{\xi},\bar{z}_n) \\ u_z(\bar{\xi},\bar{z}_{n+1}) \\ u_r(\bar{\xi},\bar{z}_{n+1}) \end{Bmatrix} \quad (3.17c)$$

$$\mathbf{K}^{(n)} = \begin{bmatrix} \mathbf{-S}^{(n)}(\bar{\xi},\bar{z}_n) - \mathbf{Z}_n(\bar{\xi},\bar{z}_n) \\ \cdots\cdots\cdots\cdots\cdots\cdots\cdots\cdots \\ \mathbf{S}^{(n)}(\bar{\xi},\bar{z}_{n+1}) \end{bmatrix} \begin{bmatrix} \mathbf{R}^{(n)}(\bar{\xi},\bar{z}_n) \\ \cdots\cdots\cdots\cdots \\ \mathbf{R}^{(n)}(\bar{\xi},\bar{z}_{n+1}) \end{bmatrix}^{-1} \quad (3.17d)$$

3.5 GLOBAL STIFFNESS MATRIX

The advantage of using technique of global stiffness matrix is that the condition number of the equation system is relatively low compared to the conventional technique [24]. To assemble the global stiffness matrix of the multi-layered elastic medium, the continuity conditions of traction and displacements at each surface are needed. From the continuity conditions in the eq. (3.11a) to (3.11c) and the relationship between the

displacements and the stresses at each layer in the eq. (3.17a), the global equation system can then be established as

$$\mathbf{K}^{*}\mathbf{U}^{*} = \mathbf{F}^{*} \tag{3.18a}$$

in which

$$\mathbf{F}^{*} = \frac{1}{2\bar{\xi}^{2}}\left[P(\bar{\xi}) \quad Q(\bar{\xi}) \quad 0 \quad 0 \quad \cdots \quad 0 \quad 0 \right]^{T} \tag{3.18b}$$

$$\mathbf{U}^{*} = \left[u_z(\bar{\xi},\bar{z}_1) \quad u_r(\bar{\xi},\bar{z}_1) \quad u_z(\bar{\xi},\bar{z}_2) \quad u_r(\bar{\xi},\bar{z}_2) \quad \cdots \quad u_z(\bar{\xi},\bar{z}_{N+1}) \quad u_r(\bar{\xi},\bar{z}_{N+1}) \right]^{T} \tag{3.18c}$$

and the matrix $\mathbf{K}^{*}$ is the global stiffness matrix established by assembling the matrix $\mathbf{K}^{(n)}$ from the eq. (3.17d) with the consideration of the continuity conditions of traction and displacements from eq. (3.11a) to (3.11c) of each surface. The functions $P(\bar{\xi})$ and $Q(\bar{\xi})$ are the Hankel transform of the normalized surface loading, i.e. $p(r)/\mu^{(1)}$ and $q(r)/\mu^{(1)}$ respectively. The solution to the above global equation system yields the Hankel transforms of the displacements at each layer interface. Hankel transforms of the stresses at the layer interfaces can then be obtained by substituting the solution to the displacements into eq. (3.17a). Finally, the displacement and stress fields can be determined by applying an accurate numerical quadrature scheme. In the next chapter, the procedure and the details of the numerical quadrature scheme are provided following by the verification of the scheme on existing solutions. Thereafter, parametric studies investigation are conducted based on practical models to study the influence of various parameter on elastic fields of the layered medium.

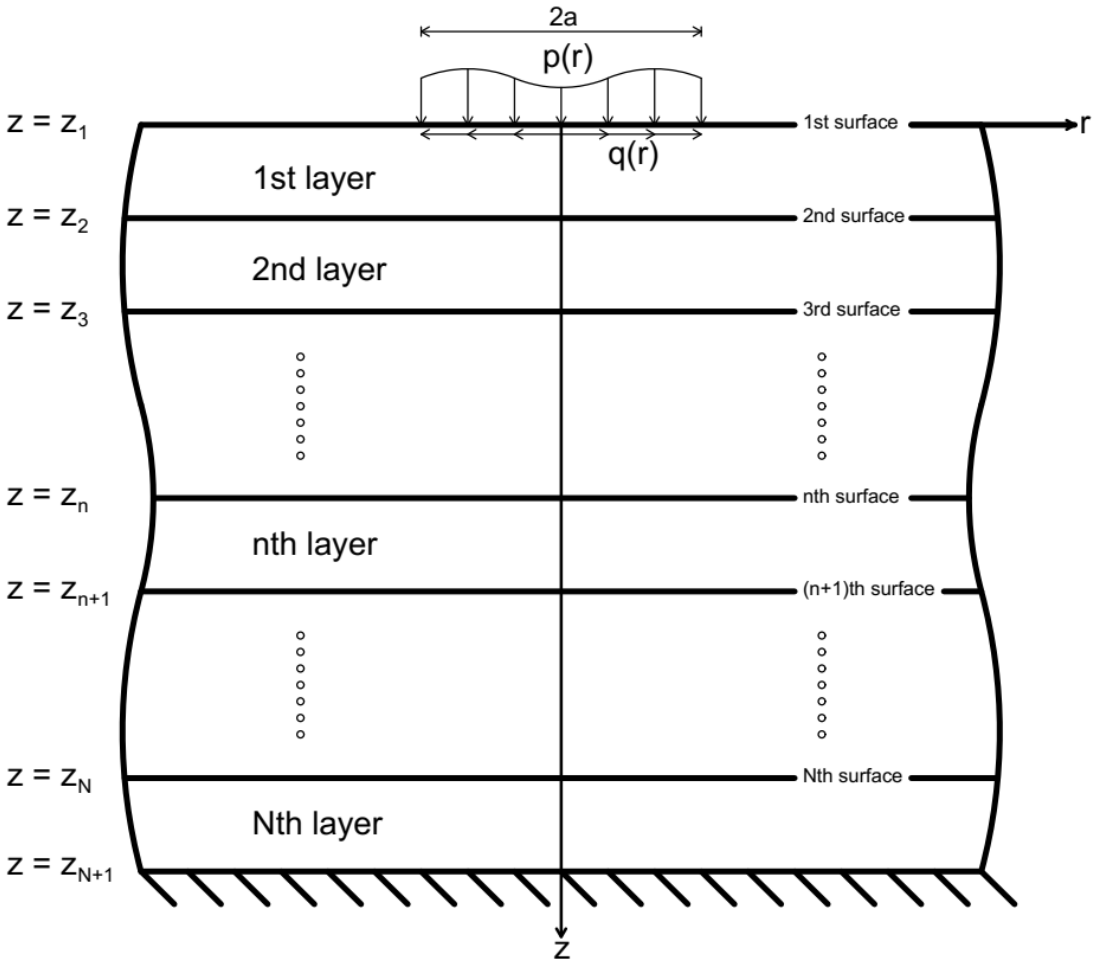

Figure 3.1. A multi-layered elastic medium over a rigid base under axisymmetric surface loading

CHAPTER IV

NUMERICAL RESULTS AND DISCUSSION

4.1 NUMERICAL SCHEME VERIFICATION

A computer code is developed based on the exact stiffness matrix scheme to evaluate the displacements and stresses of a multi-layered elastic medium with the presence of the surface energy effects. The tasks performed by the computer code follows the detail described in the section 3.4 and 3.5. First, the stiffness matrices corresponding to each layer is computed from the input parameters for specified values of Hankel transform parameter ξ. These stiffness matrices are then assembled into the global stiffness matrix form of eq. (3.18a), and the displacement vector, eq. (3.18c), is obtained by solving the global stiffness equation for each specified value of ξ. Thereafter, the displacements at the top surface and each interface are obtained by evaluating the semi-infinite integrals with respect to ξ in the displacement vector by using numerical quadrature scheme based on 21-point Gauss-Kronrod rule [34]. To obtain the stresses, the relation of stresses and displacements of the n^{th} layer shown in the eq. (3.17a) and (3.17d) have to be evaluated after the displacement vector is obtained, and the same integral process applied to the displacement is then performed on the obtained the stress solution.

Two verification models have been chosen to verify the present solution scheme. To test the scheme of elastic functionally graded layer, called FG layer, over an underlying half-space subjected to uniformly distributed loading, the solution by Katebi and Selvadurai (2013) [35] is chosen. The FG layer is modelled as a multi-layered medium with their elastic material properties vary through the layer thickness by the grading exponential function $\mu(\bar{z}) = \mu_0 e^{\bar{m}\mu_0 \bar{z}}$ where $\bar{m}$ is the grading constant and μ_0 is the shear modulus corresponding to the material of the top surface with the constant Poisson's ratio of 0.5. The FG layer is divided into a number of sublayers where each layer has the same thickness, the shear modulus within each layer is constant and it is computed at the mid-height of the layer. The appropriate number of

sublayers to represent the FG layer is studied and as the normalized thickness of the layer is 1.0, ten sublayers are acceptable, in which the error occurred from this model is less than 0.01%. To improve the accuracy, the FG layer can be divided where thickness of each layer is different corresponding to the gradient of the grading function. The properties of the remaining half-space are the same as the properties of the material at the lower surface of the layer. The half-space is modelled as 10 sublayers of elastic layers with uniform thickness of 0.1 on a relatively large elastic layer over rigid base. The medium is subjected to the internal axisymmetric uniform vertical loading applied at the interface between FG layer and homogeneous half-space. The internal loading function is expressed as the following equation

$$p(r) = p_0 H\left(a - r\right) \tag{4.1}$$

where $H\left(a-r\right)$ is the Heaviside step function, a is the loading radius and p_0 is the loading magnitude. The ratio of the layer thickness to the radius of the loading H/a is set to 1.0. The verification of the vertical displacement at the interface along the radial direction is illustrated in Figure 4.1a for the case where $\overline{m}$ = 0.25, 1.0 and 1.5, and the normal stress along the vertical direction when H/a ratio is set to 2.0 for the case when $\overline{m}$ = 0.0, 0.5 and 1.0 is presented in Figure 4.1b. Both solutions show excellent agreement with the corresponding existing solutions [35].

The second verification, with Tirapat et al. (2017) [22], is conducted by comparing with the solution for an infinite elastic layer of Si [100] over an underlying half-space of Al [111] subjected to the same loading as the first verification, applied to the top surface, with the ratio of the layer thickness to the loading radius of 1.0. The material properties and surface properties of Si [100] and Al [111] are shown in Table 4.1 [5, 36]. The upper layer of Si [100] is divided into 10 sublayers and the half-space Al [111] is also divided into 10 sublayers and a half-space to ensure the capability of the scheme to handle the multi-layered structure. In addition, the surface energy effects are considered only on the top surface and the interface, no effects on any interface between sublayers. The excellent agreement between the two solutions can be observed in both displacement and stress profiles shown in Figure 4.2a and 4.2b.

4.2 NUMERICAL SOLUTIONS

4.2.1 Multi-layered medium over rigid base

The influence of surface energy effects and the size-dependency effect have been studied in this section. The capability of the program when subjected to various loading cases is demonstrated. A model of Si/Al multi-layered medium resting on a rigid base is selected since Si/Al multi-layered structure is one of the most well-known systems for micro- and nano-electronic materials [37]. The multi-layered medium consists of two different materials stacking alternately throughout the total thickness, H. The odd layers are Si [100] and the even layers are Al [111] where the thicknesses of both layers, h_1 and h_2, are both equal to 0.2 nm. The thickness of the medium is equal to 1 μm and subjected to top surface axisymmetric loading with the loading function as shown in eq. (4.1) where the normalized thickness $\bar{a}$, a/Λ, equal to 1.0. The boundary value problem is illustrated in Figure 4.3. The material properties of Si [100] and Al [111] are shown in Table 4.1 where the surface properties of Si [100] are selected as the properties of the top surface and the surface properties of Al [111] are hypothetically selected as the properties of the other surfaces, called interfaces. From Table 4.1, the material length scale Λ of Si [100] is equal to 0.16739 nm which is used as the structure length scale to normalize every dimensional parameter. Therefore, the normalized thickness of each layer is equal to 1.195 and the loading radius is equal to 0.16739 nm. In addition, the superposed bar symbol "$\bar{}$" implies that the parameter below the symbol is normalized with the material length scale.

After all the parameters are set, then the model is ready for investigations. Figure 4.4 shows the vertical displacement and the normal stress of the Si/Al multi-layered medium at different profiles along the radial direction for the cases where the surface energy effects are considered and ignored. The monitoring profiles for the displacement are the top surface where z = 0.0 nm, the second surface where z = 0.2 nm and the third surface where z = 0.4 nm while for the stress, the same set of monitoring profiles are used except for the first profile, a profile of the middle of the first layer where z = 0.1 nm is used instead. It can be implied from the results that the influence of the surface energy effects is significant to the vertical displacement and

normal stress at all profiles shown in Figure 4.4, especially the profile at the depth close to the top surface where the loading is applied.

Moving onto the study of influence of the surface energy effects at the interface, since the surface elastic properties of the interfaces between two specific materials are still not defined yet, the investigation on the influence at the interfaces by varying the surface elastic properties at each interface is beneficial. The residual surface stress of the interfaces τ_2^s is varied whereas the residual surface stress of the top surface τ_1^s remain the same. The results, displacements at the top surface and stresses at the profile z = 0.1 nm, are obtained with the ratio of the residual surface stress of the interface to the top surface, τ_R, being -0.5, 1.0, 2.0 and 5.0 while the value of κ^s remains the same for all cases. The similar trends can be observed in all the results shown in Figure 4.5, i.e. the value at every points of all the results converged to zero when the ratio increases. This means that the increment of the effects renders the medium stiffer than those with lesser value of the τ_R ratio, and the residual surface stress at every interface contributes significantly to the results in this model. Note that the surface elastic constant κ^s contributes negligible influence on the results compared to the residual surface stress τ^s [17].

Although the size dependency effect has been studied by various researchers, the effect on a multi-layered medium is the topic that has not been discussed yet. The numerical experiments have been conducted on a default model to obtain vertical displacement and normal stress at the depth of z = 0.0 nm for the displacement, z = 0.1 nm for the stress and $\bar{r}/\bar{a}$ = 0.5 for both fields while varying the parameter $\bar{a}$. The ratio $\bar{H}/\bar{a}$ is kept constant for every $\bar{a}$. The influence of the size dependency effect is illustrated in Figure 4.6 which indicates the trend of the elastic fields when the parameter $\bar{a}$ is changed. The differences between the elastic fields with the surface energy effects and without the effects are reduced when $\bar{a}$ is increased. However, the differences are significant when the value of $\bar{a}$ is small, approximately below 2.0. Additionally, the results of the present study do agree well with the work from Rungamornrat et al. [18].

The capability of the numerical scheme in terms of applied loading cases is also investigated in this study. Three different types of axisymmetric loading cases are chosen with the same amount of total force, namely, uniformly distributed vertical loading as shown in eq. (4.1), the contact pressure from the flat-ended rigid punch and the contact pressure from the paraboloid revolutionary rigid punch. The second and third loading cases are the assumed forms of loading function which provides the similar contact pressure to flat-ended rigid punch and paraboloid revolutionary rigid punch indentation problem respectively when applied to the homogeneous half-space medium. The assumed form of loading function of the flat-ended rigid punch is expressed in the following equation[38]

$$\bar{p}(\bar{r}) = (p_0 / \mu^{(1)}\bar{a}) / \sqrt{(1-(\bar{r}/\bar{a})^2)}H(\bar{a}-\bar{r}) \tag{4.2a}$$

and the assumed form of loading function for paraboloid revolutionary case [38] is

$$\bar{p}(\bar{r}) = (p_0 / \mu^{(1)}\bar{a})\sqrt{(1-(\bar{r}/\bar{a})^2)}H(\bar{a}-\bar{r}) \tag{4.2b}$$

where $H(\bar{a}-\bar{r})$ is the Heaviside step function. The vertical displacement of the top surface and the normal stress at the profile z = 0.1 nm are plotted in Figure 4.7. The vertical displacement of the flat ended and paraboloid revolutionary cases shown in Figure 4.7 reflects the flat and paraboloid shapes respectively. The influence of surface energy effects can be found on all results corresponding to the three loading cases. The flat ended loading case provides the maximal displacement whereas the paraboloid revolutionary case provides the minimal. On the stress result, the influence of the surface energy effects is significant only under the contact area of the loading where $\bar{r}/\bar{a} \le 1.0$.

4.2.2 Functionally graded elastic medium

The second model is a model of functionally graded layer on a homogeneous elastic medium overlying a rigid based. The elastic properties of the FG layer vary in

the z-direction from the elastic properties of Si [100] at the depth $\bar{z} = 0.0$ to the elastic properties of Al [111] at the depth $\bar{z} = \bar{h}_1$ where $\bar{h}_1$ is the normalized thickness of the FG layer as shown in Figure 4.8. The variational pattern of the elastic properties of the FG layer is determined by the grading function in which the exponential function, $L(\bar{z}) = L_0 e^{\bar{m} L_0 \bar{z}}$ where $\bar{m}$ is the grading constant and L_0 is the Lame' constants of Si [100], is selected for every cases of this model. The value of the grading constant $\bar{m}$ is obtained by back calculation from the known elastic properties at the depth $\bar{z} = 0.0$ and $\bar{z} = \bar{h}_1$. The FG layer is divided into 10 sublayers where the elastic properties of each layer are assigned in the same manner as the verification model. The underlying homogeneous elastic layer is a layer of Al [111] and its layer thickness is equal to h_2. The $\bar{h}_2 / \bar{h}_1$ ratio is set to 9.0 where the ratio $\bar{H} / \bar{a}$ and the loading radius $\bar{a}$ are both set to 1.0. This model is subjected to the same loading case as the multi-layered model, eq. (4.1). The surface elastic properties of the top surface and the interface of this model are equal to the surface properties of Si [100] and Al [111] respectively.

The top surface vertical displacement corresponding to the variation of the thickness ratio between upper and lower layer are illustrated in Figure 4.9 with $\bar{H} / \bar{a}$ being fixed at 1.0. Since Al [111] has lower elastic properties than Si [100], the obtained displacement then becomes maximal when the thickness of Al [111] is 9.0, which is the largest thickness considered in the Figure 4.9.

Studying the influence of the total thickness H on the top surface vertical displacement of the FG layer model when the total thickness is increased whereas the first layer thickness remains the same is presented in Figure 4.10. As the thickness increases, the influence of the surface energy effects increases.

The vertical displacement profiles along the radial direction at each profile through the thickness of the multi-layered medium have been plotted to study the surface energy influence as the distance between the selected profiles and the top surface increases. The results illustrated in Figure 4.11 can be implied in the same way as the multi-layered model, i.e. the influence of the surface energy effects on the

displacement is lower when the distance between the profile and the top surface increases.

Turning to investigate the effect of the residual surface stress τ^s on the FG layer problem. Figure 4.12 shows the displacements profiles at the top surface and the stresses profiles at the interface between the FG layer and the homogeneous layer with the value of τ_R being -0.5, 1.0, 2.0 and 5.0. The similar trend to the Si/Al multi-layered model can be observed in Figure 4.12 where the presence of the residual surface stress increases the stiffness of the elastic medium.

Another point of interest is the influence of grading function to the solutions. To investigate the difference between the grading function of the FG layer, three grading functions, namely, linear, exponential and power law distributed grading function, have been employed to observe the variation of the top surface vertical displacement and normal stress at the interface. The linear and power law distributed grading function can be expressed as $L(\bar{z}) = L^{(1)}(1+m\bar{z})$ where $m = (L^{(N)} - L^{(1)})/(L^{(1)}\bar{h}_1)$ and $L(\bar{z}) = L^{(1)}(1+\bar{z}/\bar{h}_1)^m$ where $m = \log_2(L^{(N)}/L^{(1)})$ respectively when $\bar{z} \le \bar{h}_1$. The special case of the FG layer has been introduced to emphasize the difference between the results among gradation functions. The elastic properties of the top surface and the interface, previously assigned as the properties of Si [100] and Al [111] respectively, are substituted by the 1st material and the 2nd material for this special case, which are μ_1 = 100 GPa, λ_1/μ_1 = 1.5 for the 1st material and μ_2 = 10 GPa, λ_2/μ_2 = 1.5 for the 2nd material. The ratio $\bar{h}_2/\bar{h}_1$ for this special case is set to 1.5, the thickness $\bar{h}_1$ is 0.4, the ratio $\bar{H}/\bar{a}$ is kept to 1.0 and the surface quantities at the top surface and the interface remain unchanged from the FG model. The results show that the stiffest grading function is the linear distribution, followed by the exponential and the power law respectively as shown in Figure 4.13. However, the results also show that the selection of grading function is significant only for the extreme cases where the variation of elastic properties and the thickness is large enough.

4.3 APPLICATIONS OF FUNDAMENTAL SOLUTIONS

The obtained results from the previous sections are based on a multi-layered medium configuration over a rigid base subjected to some cases of axisymmetric surface loading. However, many practical problems can also be handled by this calculation scheme. In the aspect of the applied loading, the scheme allows the user to analyze problems subjected to any arbitrary axisymmetric loading by simply plug-in the loading in their Hankel transform space into the numerical scheme. The loading cases in the Hankel transform space that have been frequently used are a concentrated point load $\bar{P}(\bar{\xi}) = p_0/2\pi$ with the loading magnitude of p_0, a concentrated ring load $\bar{P}(\bar{\xi}) = p_0 J_0(\bar{\xi}\bar{a})/2\pi$ where $\bar{a}$ is the radius of the ring loading, and the uniform annular load by making use of the superposition method of two uniformly distributed loading[32]. The other types of loading, including tangential loading, in the Hankel transform space can also be obtained by the method of inversion from the known function. Those loading cases can be applied on various situations such as when the medium is contacted by tubular elements, when the friction is considered, or when it is subjected to other complex form of pressure. Another aspect is that the scheme can be used to analyze boundary value problems where the loading is applied to the interface instead of surface, and the loading can also be applied to multiple interfaces or top surface with different loading functions at once. This can be useful in the further applications when there are some practical applications, which is related to the internal loading in the nano-scale systems or some macro-scale problems related to soft elastic solids.

Furthermore, the present solution can be extended to deal with the nano indentation problems. By attaching an additional indentation computational scheme to the calculation procedure to compute mixed boundary value problems, the top surface contact pressure can be generated, and the results of the boundary value problem can be obtained by the numerical scheme presented in this study afterward. This development will be a huge improvement since indentation techniques have been employed in practice to solve numerous problems, for instance, arbitrary punch profile indentation problems [38]; or using indentors for depth-sensing indentation tests to measure mechanical properties in nano-scale [39].

Table 4.1: Material properties of Si [100] and Al [111] ([5, 10, 36])

Material parameters	*Si [100]*	*Al [111]*
λ *[GPa]*	*78.0849*	*58.1700*
μ *[GPa]*	*40.2256*	*26.1300*
λ^s *[N/m]*	*4.4939*	*6.8511*
μ^s *[N/m]*	*2.7779*	*-0.3760*
τ^s *[N/m]*	*0.6056*	*0.9108*
κ^s *[N/m]*	*10.0497*	*6.0991*
Λ *[nm]*	*0.16739*	*0.15288*

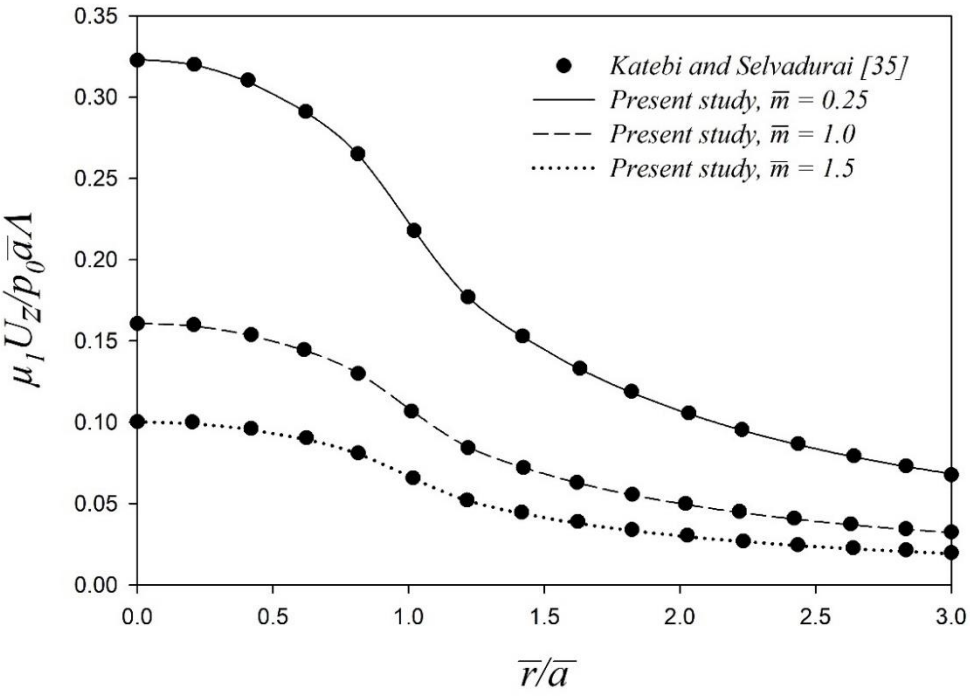

(a)

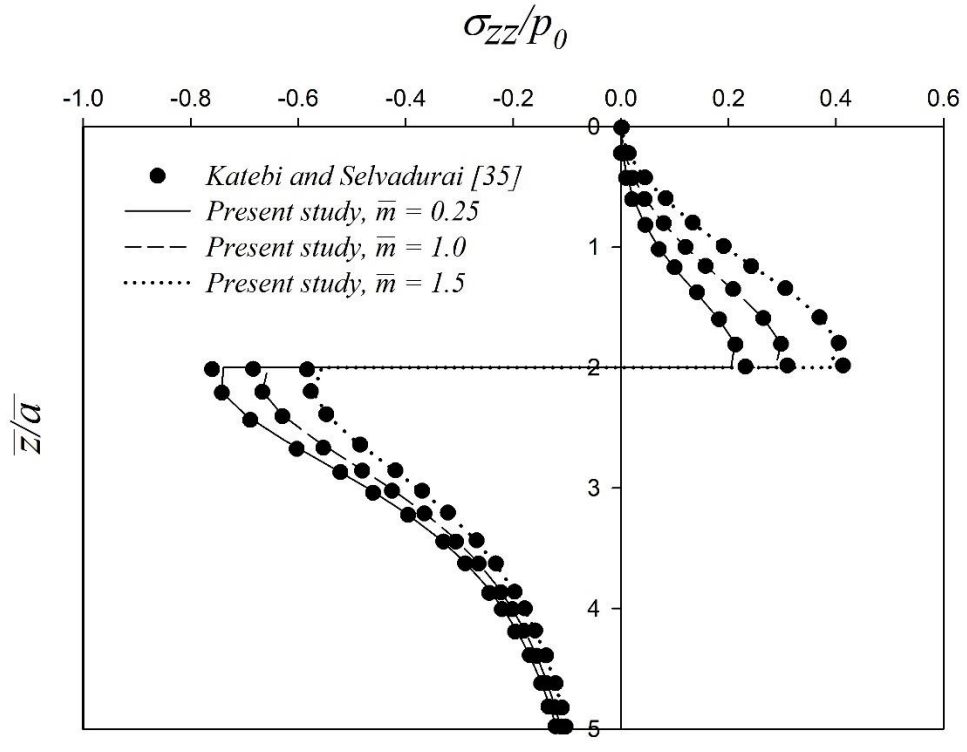

(b)

Figure 4.1. Comparison of (a) normalized vertical displacement profiles at the interface; and (b) normalized normal stress profiles along the z-axis of a FG layer over an elastic half-space

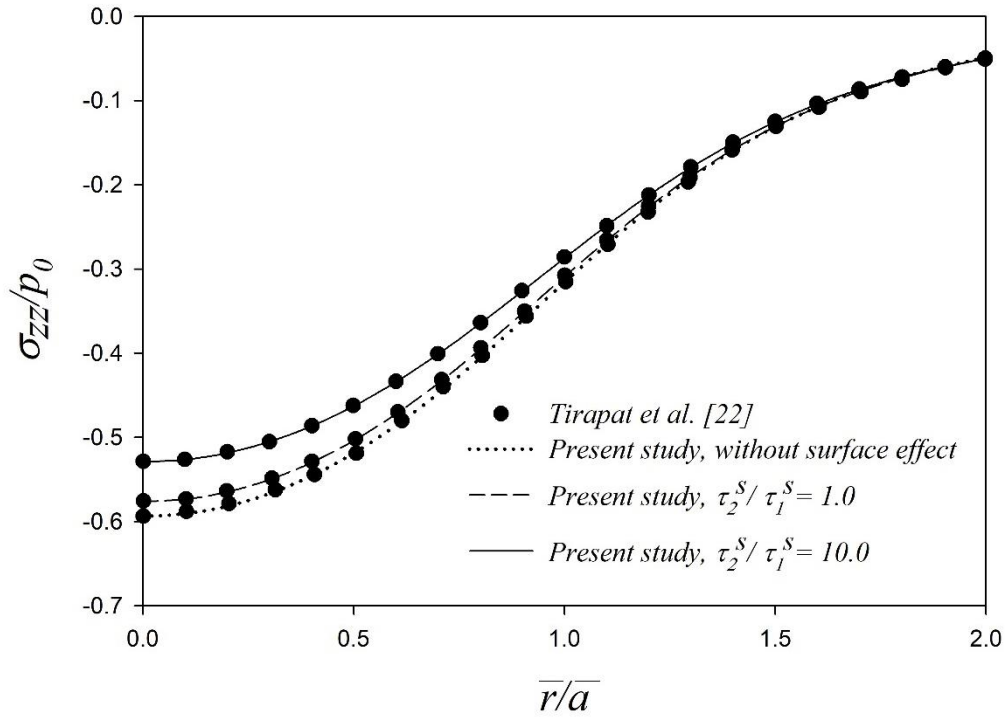

(a)

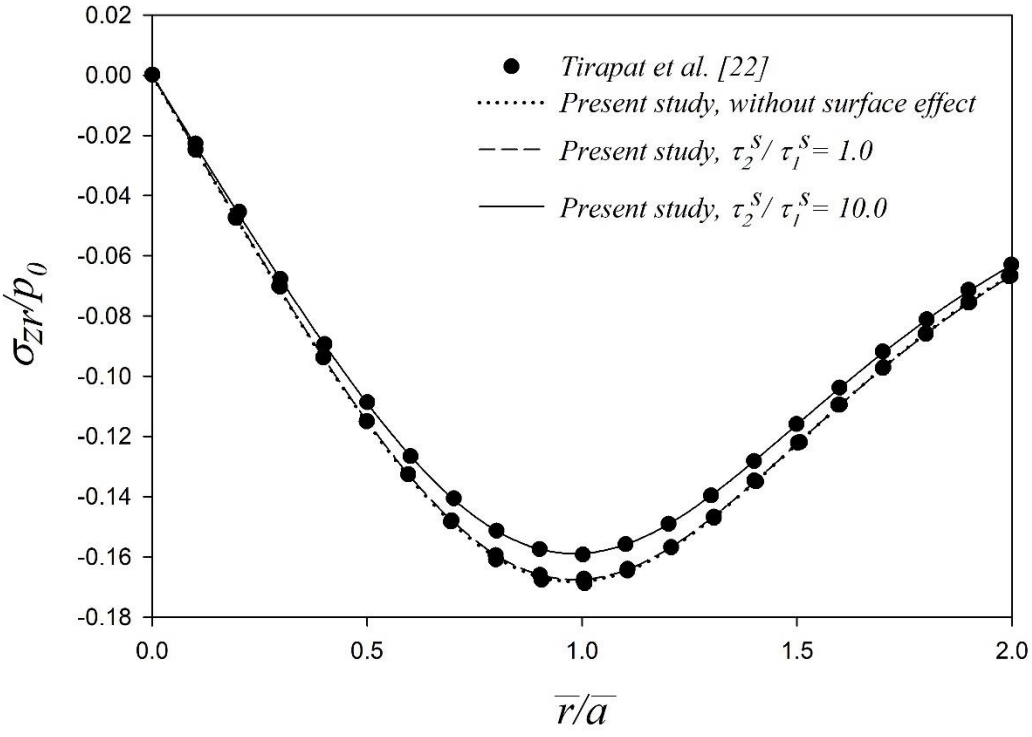

(b)

Figure 4.2. Comparison of radial profiles of (a) normalized normal stress; and (b) normalized shear stress of a layer elastic half-space with the influence of surface energy effects

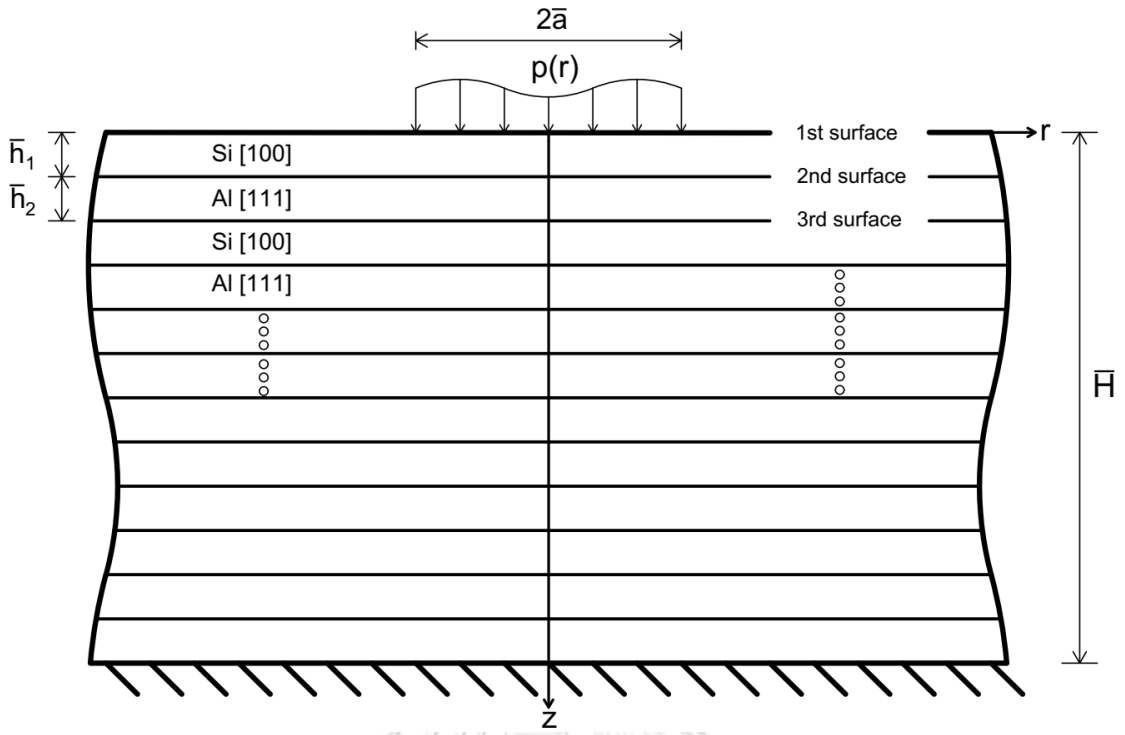

Figure 4.3. A multi-layered medium consisting of Si [100] and Al [111] under vertical surface loading

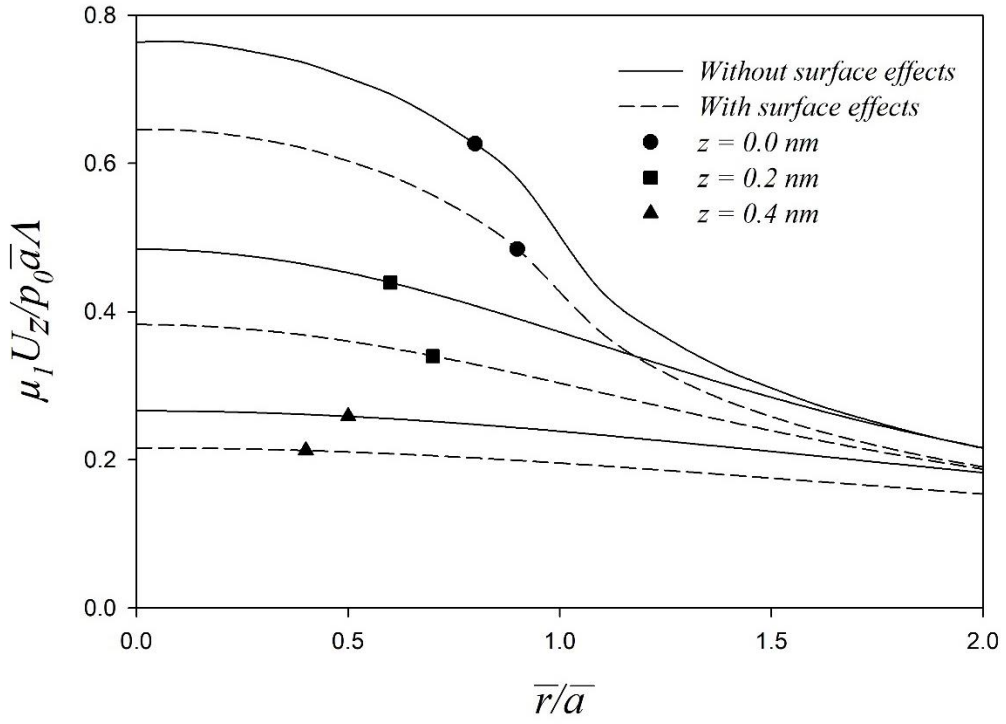

(a)

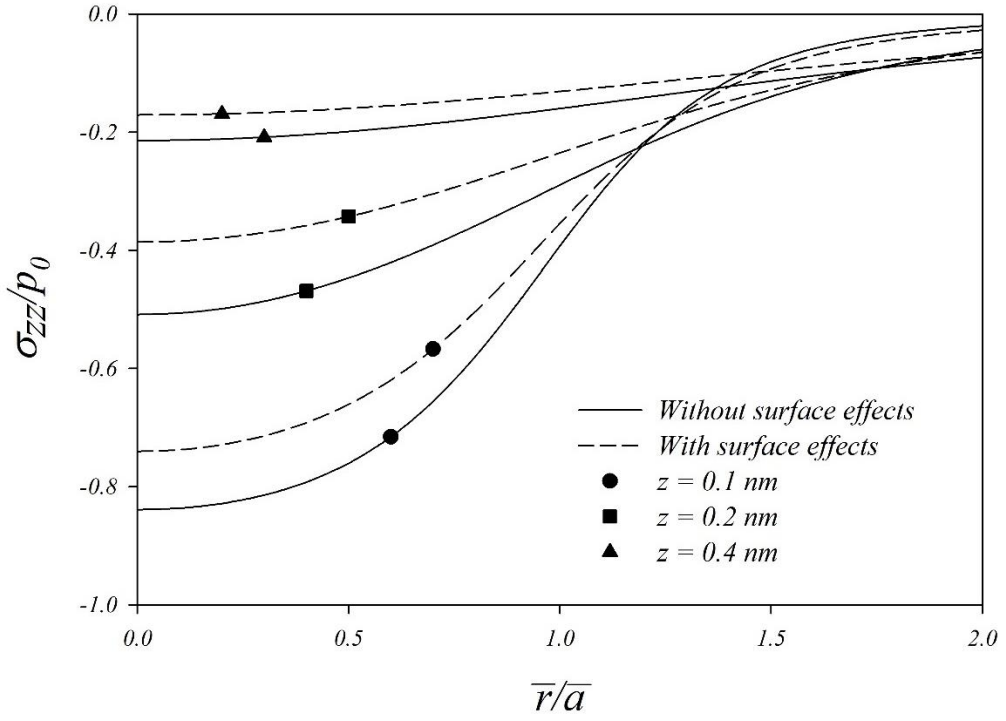

(b)

Figure 4.4. Radial profiles of elastic fields of the Si/Al multi-layered medium at defferent depths: (a) normalized vertical displacement; and (b) normalized normal stress

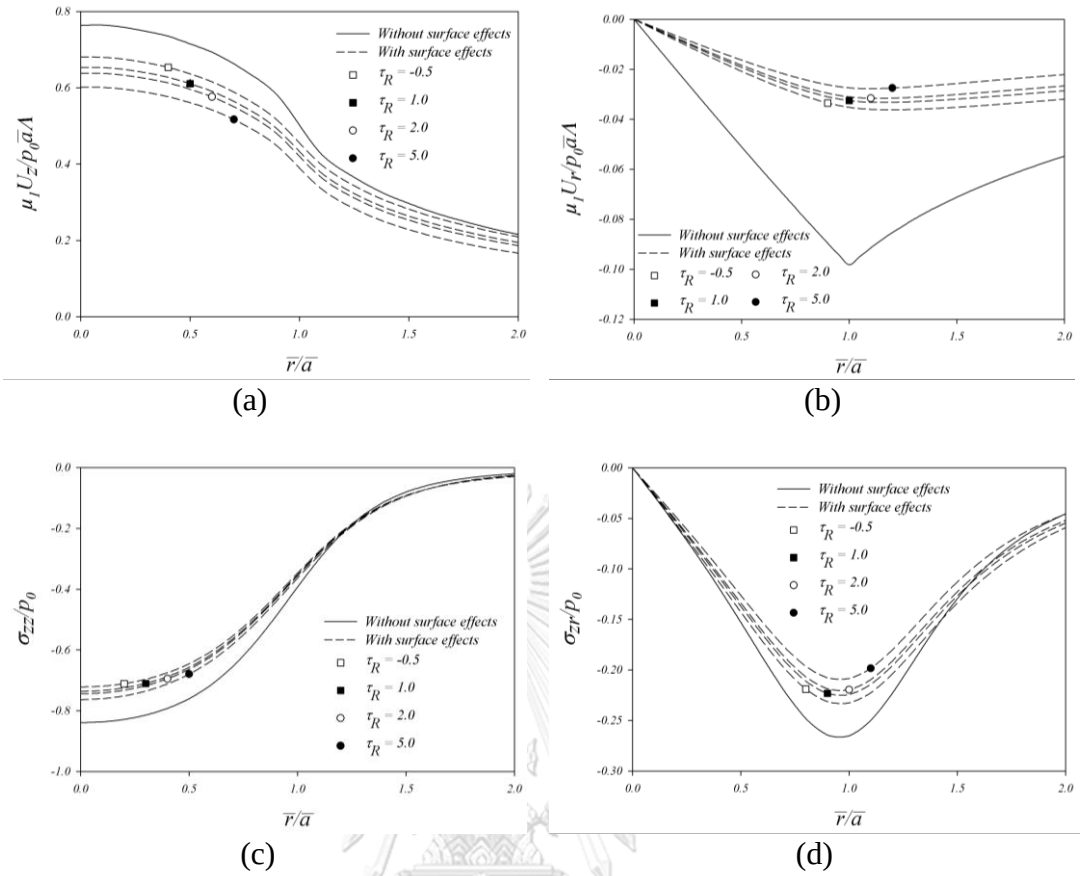

Figure 4.5. Radial profiles of elastic fields of the Si/Al multi-layered medium with different τ_R ratios: (a) normalized vertical surface displacement; (b) normalized radial surface displacement; (c) normalized normal stress at z = 0.1 nm; (d) normalized shear stress at z = 0.1 nm

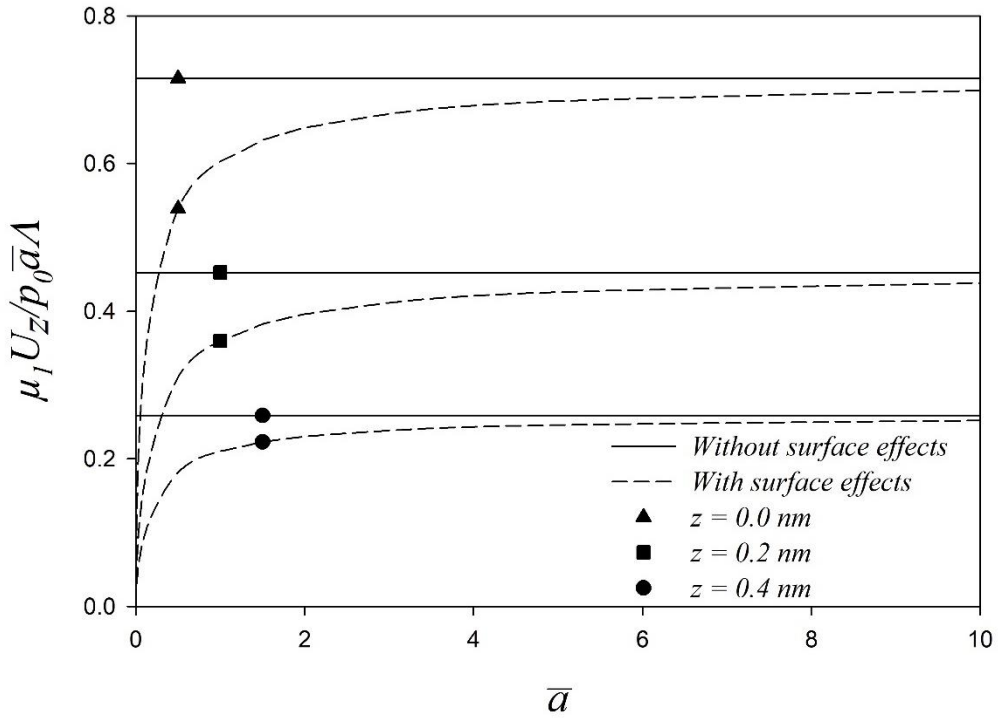

(a)

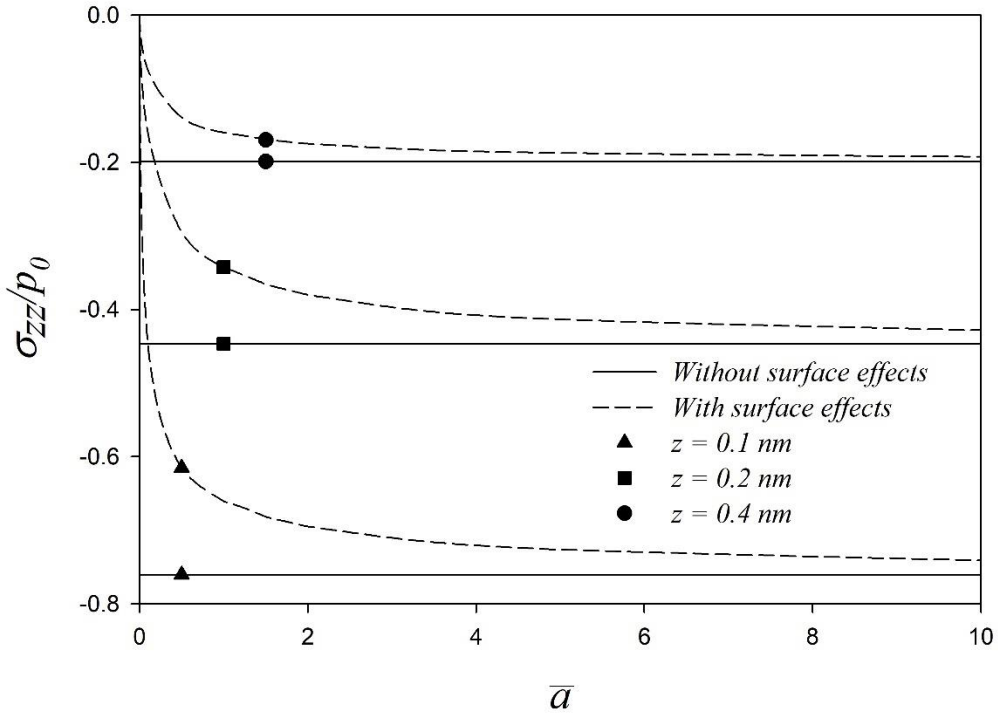

(b)

Figure 4.6. Variation of elastic fields of the Si/Al multi-layered medium with normalized loading radius $\bar{a}$ at different depths: (a) normalized vertical displacement; (b) normal stress

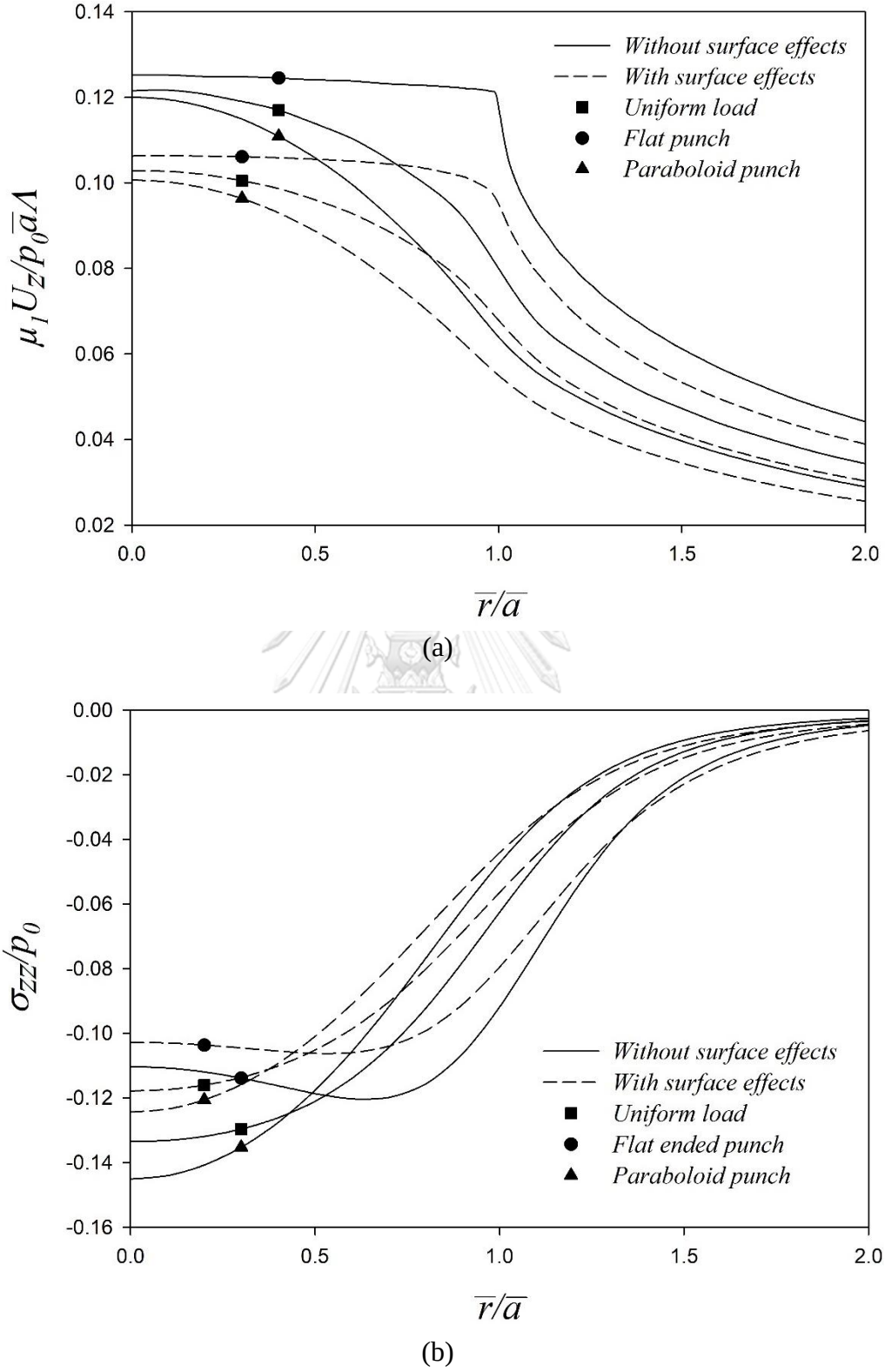

Figure 4.7. Radial profiles of elastic fields of the Si/Al multi-layered medium under different types of surface loading: (a) normalized vertical surface displacement; and (b) normalized normal stress at z = 0.1 nm

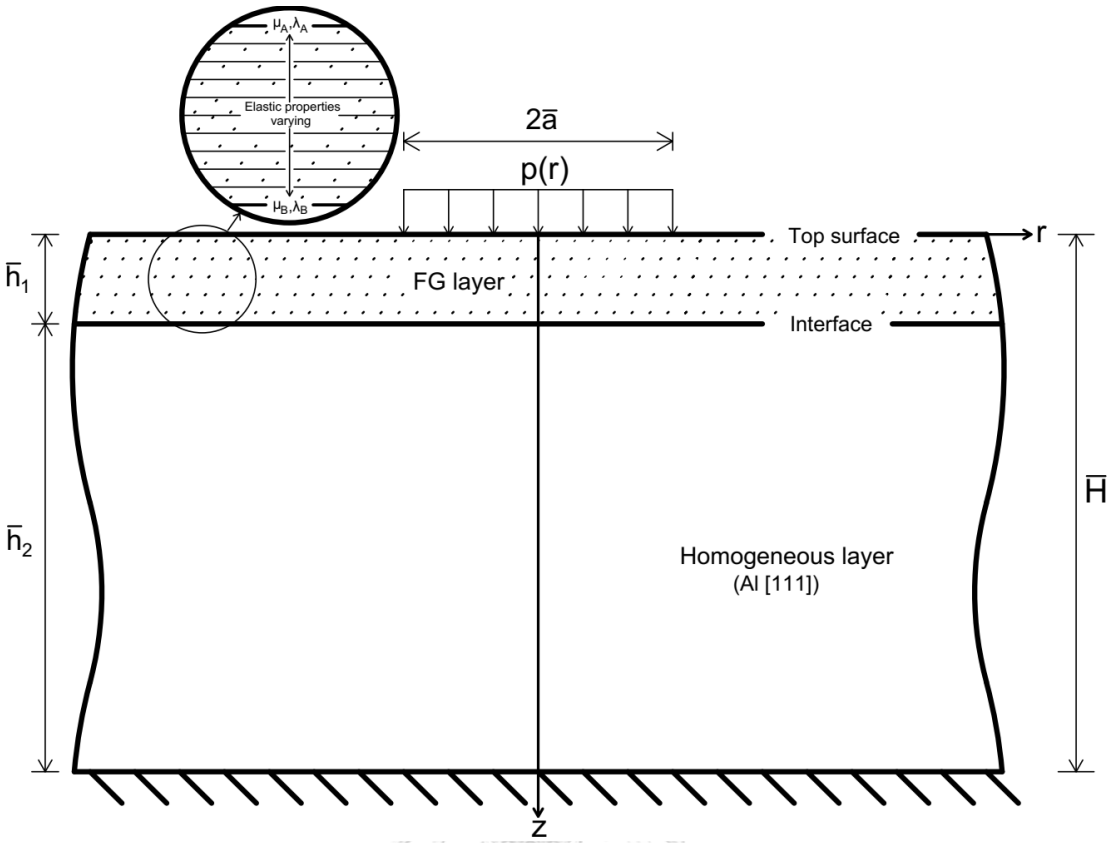

Figure 4.8. A FG layer over an elastic medium under uniform vertical surface loading

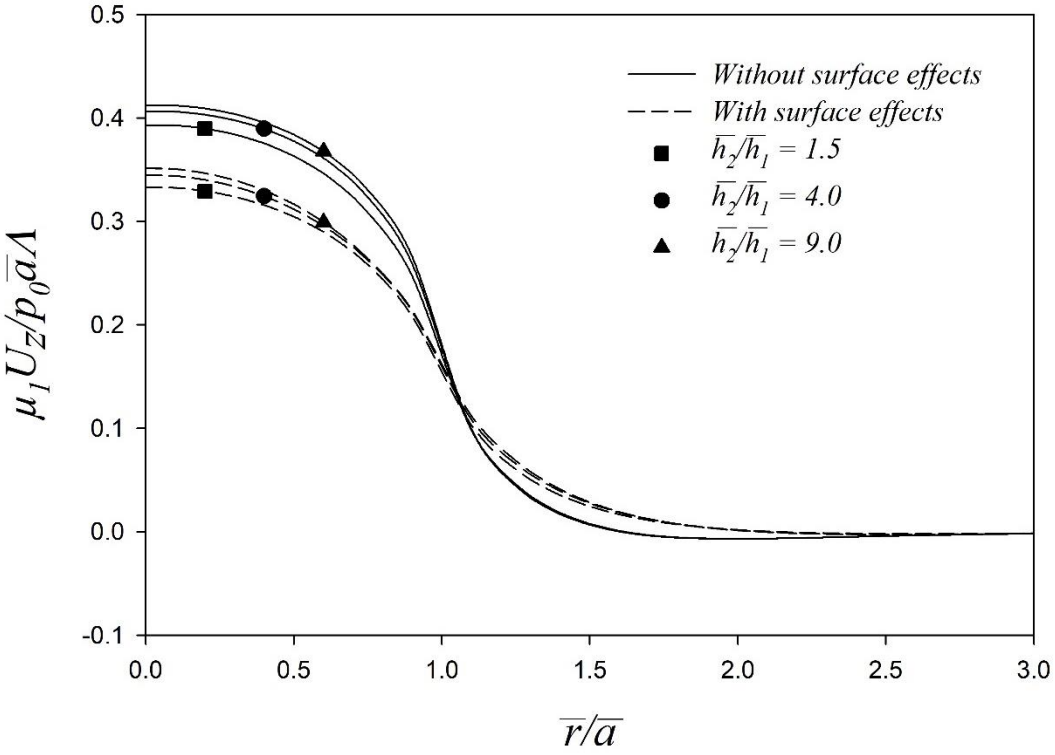

Figure 4.9. Radial profiles of normalized vertical surface displacement of the FG elastic medium with different $\bar{h}_2 / \bar{h}_1$ ratios

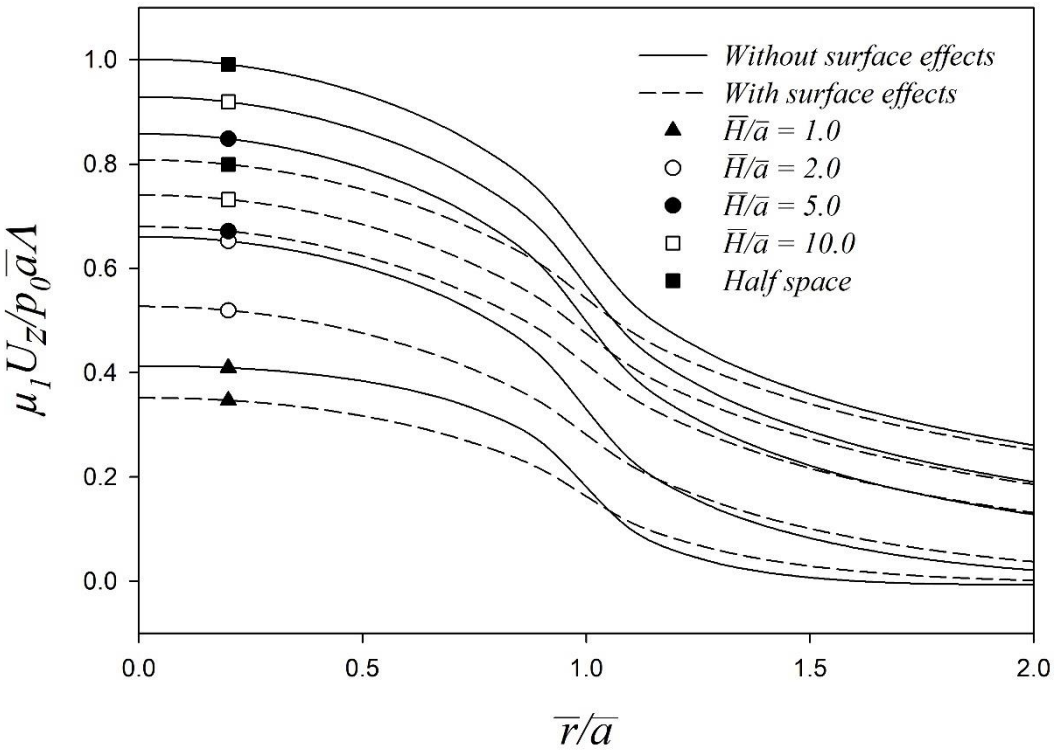

Figure 4.10. Radial profiles of normalized vertical surface displacement of the FG elastic medium with different $\overline{H}/\overline{a}$ ratios

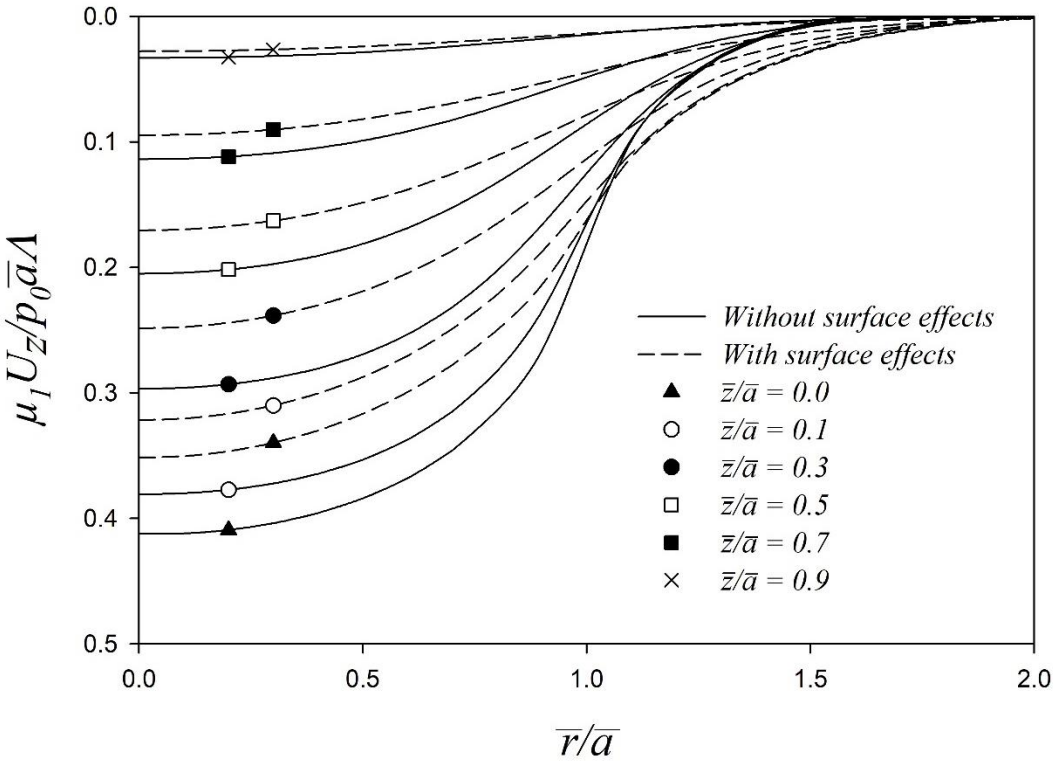

Figure 4.11. Radial profiles of normalized vertical displacement of the FG elastic medium at different depths

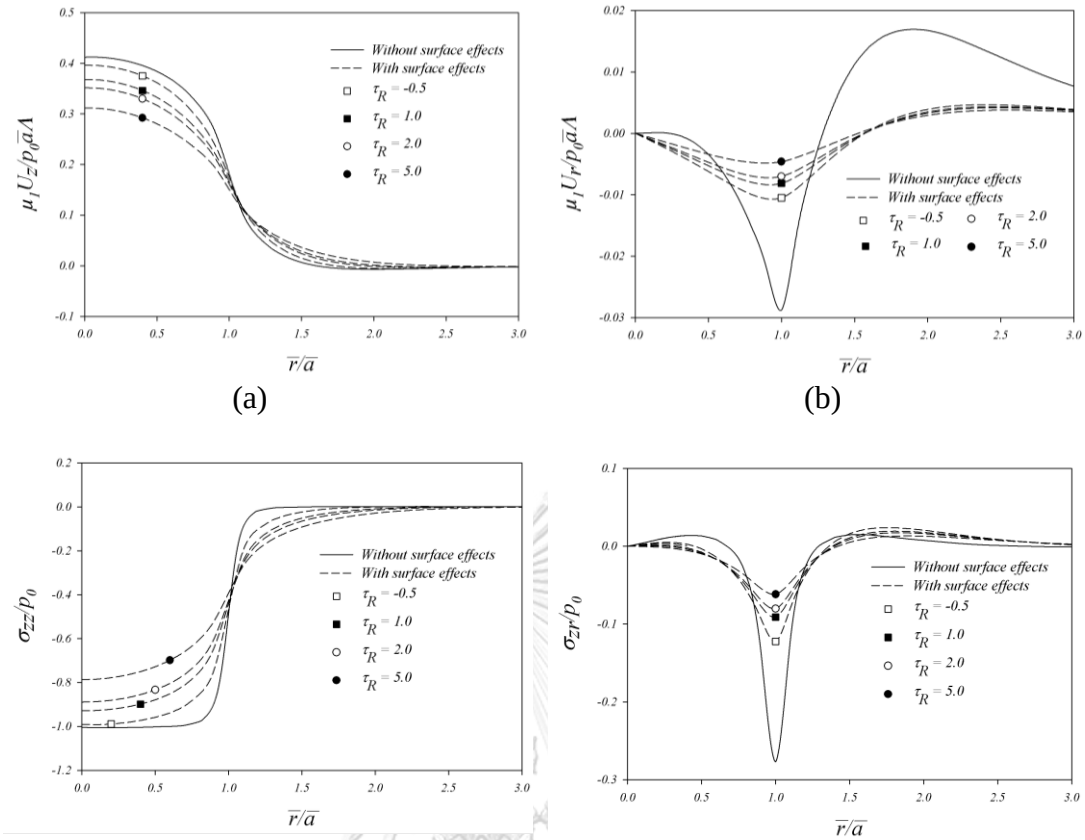

Figure 4.12. Radial profiles of elastic fields of the FG elastic medium with different τ_R ratios: (a) normalized vertical surface displacement, (b) normalized radial surface displacement; (c) normalized normal stress at the interface, (d) shear stress at the interface

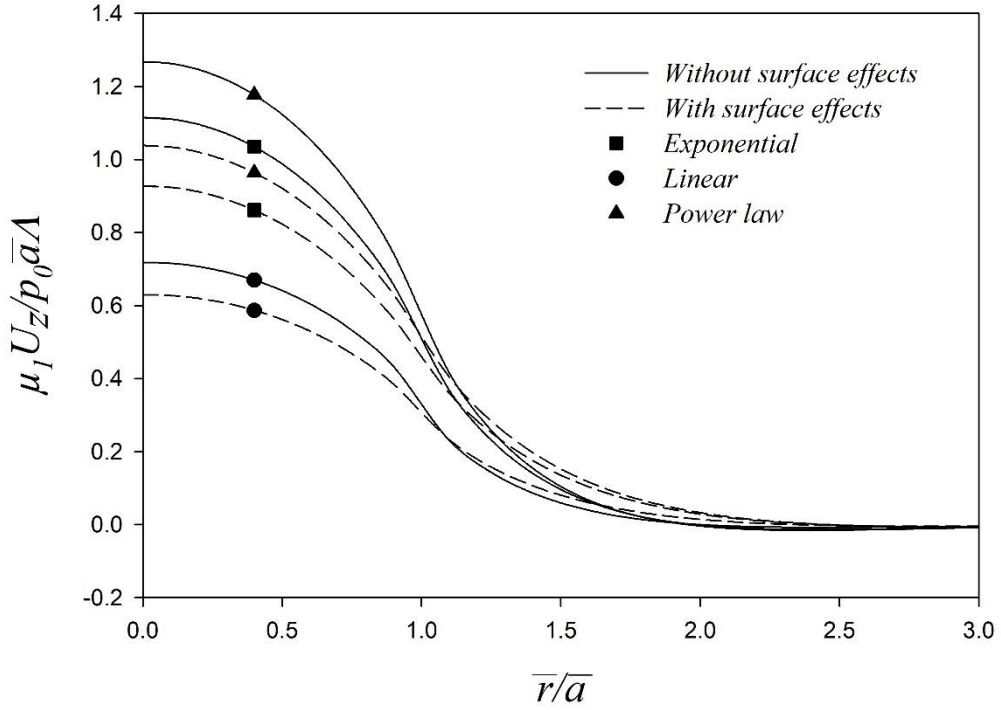

(a)

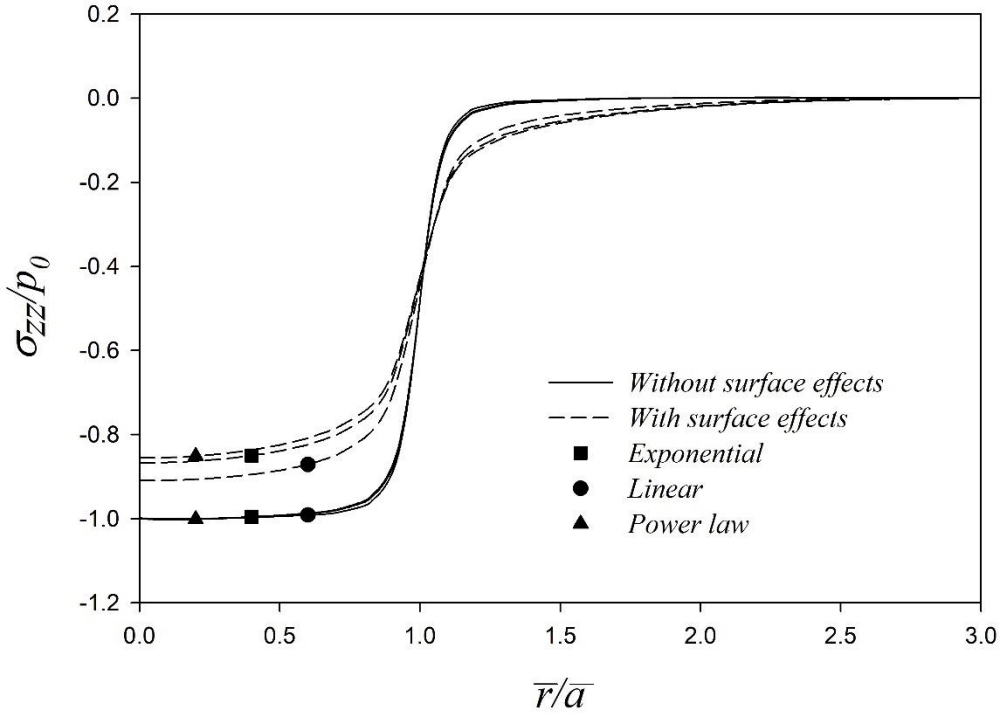

(b)

Figure 4.13. Radial profiles of elastic fields of the FG elastic medium with different grading functions: (a) normalized vertical surface displacement; and (b) normalized normal stress at the interface

CHAPTER V

CONCLUSION

The mathematical model for solving a multi-layered elastic medium, with consideration of the surface energy effects, and subjected to axisymmetric loading is developed in this study. The standard Love's representation and the Hankel integral transform are adopted to obtain general solutions of each layers, which are assembled and numerically solved by the exact stiffness matrix method. To capture the surface energy effects, the surface elasticity theory by Gurtin-Murdoch is adopted. The parametric studies have been carried out for two models, a multi-layered medium over a rigid base and a functionally graded elastic medium with the intentions to portray the capabilities of the calculation scheme on different multi-layered models and to study the influence of the surface energy effects on elastic fields of the layered medium.

The numerical results show that, apart from numerous uses of the multi-layered scheme presented in previous works, this scheme can handle the multi-layered problems or functionally graded problem with the presence of the surface energy effects, in which the value of surface elastic properties of the top surface and each interface can be assigned individually. The results indicate that the surface elastic properties, especially the residual surface stress, of the top surface and interfaces have a great influence on both displacement and stress results. The results also indicate that the residual surface stress of the same surface as the loading plane, i.e. the top surface, has the most impact on the results compared to that of the interfaces. Other parameters can also affect the influence of the surface energy effects as well, for instance, the loading radius and the elastic material properties. The outcomes of this study can be used in various ways, for instance, the present solution can be used as benchmark solutions in the development of numerical approaches such as FEM and BEM for the analysis of multi-layered structures with the influence of surface energy effects This solution scheme can be further modified to analyze other practical multi-layered systems with the surface energy effects such as indentation problems.

REFERENCES

[1] P. C. Lacaze, *Nanotechnologies: Concepts, Production and Applications*. Wiley, 2012.

[2] E. W. Wong, P. E. Sheehan, and C. M. Lieber, *Nanobeam Mechanics: Elasticity, Strength, and Toughness of Nanorods and Nanotubes*. 1997.

[3] M. E. Gurtin and A. I. Murdoch, "A Continuum Theory of Elastic Material Surfaces," *Archive for Rational Mechanics and Analysis,* vol. 57, pp. 291-323, 1975.

[4] M. E. Gurtin and A. I. Murdoch, "Surface stress in solids," *International Journal of Solids and Structures,* vol. 14, no. 6, pp. 431-440, 1978.

[5] R. E. Miller and V. B. Shenoy, "Size-dependent elastic properties of nanosized structural elements," *Nanotechnology,* vol. 11, p. 139, 2000.

[6] J. W. Gibbs, H. A. Bumstead, and R. G. Van Name, *Scientific Papers of J. Willard Gibbs, Volume 1*. Longmans, Green and Company, 1906.

[7] R. C. Cammarata, "Surface and interface stress effects in thin films," *Progress in Surface Science,* vol. 46, no. 1, pp. 1-38, 1994.

[8] W. A. Goddard, D. Brenner, S. E. Lyshevski, and G. J. Iafrate, *Handbook of Nanoscience, Engineering, and Technology*. CRC Press, 2002.

[9] L. H. He and C. W. Lim, "Surface Green function for a soft elastic half-space: Influence of surface stress," *International Journal of Solids and Structures,* vol. 43, no. 1, pp. 132-143, 2006.

[10] V. B. Shenoy, "Atomistic calculations of elastic properties of metallic fcc crystal surfaces," *Physical Review B,* vol. 71, no. 9, 2005.

[11] R. D. Mindlin, "Micro-structure in linear elasticity," *Archive for Rational Mechanics and Analysis,* vol. 16, no. 1, pp. 51-78, 1964.

[12] X. L. Gao and M. Q. Liu, "Strain gradient solution for the Eshelby-type polyhedral inclusion problem," *Journal of the Mechanics and Physics of Solids,* vol. 60, no. 2, pp. 261-276, 2012.

[13] L. Tian and R. K. N. D. Rajapakse, *Analytical Solution for Size-Dependent Elastic Field of a Nanoscale Circular Inhomogeneity*. 2007.

[14] L. H. He, C. W. Lim, and B. S. Wu, "A continuum model for size-dependent deformation of elastic films of nano-scale thickness," *International Journal of Solids and Structures,* vol. 41, no. 3, pp. 847-857, 2004.

[15] P. Lu, L. H. He, H. P. Lee, and C. Lu, "Thin plate theory including surface effects," *International Journal of Solids and Structures,* vol. 43, no. 16, pp. 4631-4647, 2006.

[16] Y. Pinyochotiwong, J. Rungamornrat, and T. Senjuntichai, "Rigid frictionless indentation on elastic half space with influence of surface stresses," *International Journal of Engineering Science,* vol. 71, pp. 15-35, 2013.

[17] P. I. Intarit, "Solutions of Elastic Medium with Surface Stress Effects," Ph.D., Department of Civil Engineering, Faculty of engineering, Chulalongkorn University, 2012.

[18] J. Rungamornrat, P. Tuttipongsawat, and T. Senjuntichai, "Elastic layer under axisymmetric surface loads and influence of surface stresses," *Applied Mathematical Modelling,* vol. 40, no. 2, pp. 1532-1553, 2016.

[19] T. B. Nguyen, J. Rungamornrat, and T. Senjuntichai, "Analysis of planar cracks in 3D elastic media with consideration of surface elasticity," *International Journal of Fracture,* vol. 202, no. 1, pp. 51-77, 2016.
[20] P. Intarit, T. Senjuntichai, J. Rungamornrat, and R. K. N. D. Rajapakse, "Penny-shaped crack in elastic medium with surface energy effects," *Acta Mechanica,* vol. 228, no. 2, pp. 617-630, 2017.
[21] Y. Sapsathiarn and R. K. N. D. Rajapakse, *Finite-Element Modeling of Circular Nanoplates*. 2013, pp. 59-66.
[22] S. Tirapat, T. Senjuntichai, and J. Rungamornrat, "Influence of Surface Energy Effects on Elastic Fields of a Layered Elastic Medium under Surface Loading," *Advances in Materials Science and Engineering,* vol. 2017, pp. 1-11, 2017.
[23] Z. Gürdal, R. T. Haftka, and P. Hajela, *Design and Optimization of Laminated Composite Materials*. Wiley, 1999.
[24] T. Senjuntichai and R. K. N. D. Rajapakse, "Exact stiffness method for quasi-statics of a multi-layered poroelastic medium," *International Journal of Solids and Structures,* vol. 32, no. 11, pp. 1535-1553, 1995.
[25] R. K. N. D. Rajapakse and T. Senjuntichai, "Dynamic response of a multi-layered poroelastic medium," *Earthquake Engineering & Structural Dynamics,* vol. 24, no. 5, pp. 703-722, 1995.
[26] T. Senjuntichai and Y. Sapsathiarn, "Forced Vertical Vibration of Circular Plate in Multilayered Poroelastic Medium," *Journal of Engineering Mechanics,* vol. 129, no. 11, pp. 1330-1341, 2003.
[27] N. A. Haskell, "The dispersion of surface waves on multilayered media," *Bulletin of the Seismological Society of America,* vol. 43, no. 1, pp. 17-34, 1953.
[28] X. Y. Zhu, X. J. Liu, R. L. Zong, F. Zeng, and F. Pan, "Microstructure and mechanical properties of nanoscale Cu/Ni multilayers," *Materials Science and Engineering: A,* vol. 527, no. 4, pp. 1243-1248, 2010.
[29] W. Kern and K. K. Schuegraf, "1 - Deposition Technologies and Applications: Introduction and Overview A2 - Seshan, Krisna," in *Handbook of Thin Film Deposition Processes and Techniques (Second Edition)*Norwich, NY: William Andrew Publishing, 2001, pp. 11-43.
[30] Y. Z. Povstenko, "Theoretical investigation of phenomena caused by heterogeneous surface tension in solids," *Journal of the Mechanics and Physics of Solids,* vol. 41, no. 9, pp. 1499-1514, 1993.
[31] Z. Q. Wang, Y. P. Zhao, and Z. P. Huang, "The effects of surface tension on the elastic properties of nano structures," *International Journal of Engineering Science,* vol. 48, no. 2, pp. 140-150, 2010.
[32] I. N. Sneddon, *Fourier Transform*. New York: McGraw-Hill, 1951.
[33] Y. Wang and R. K. N. D. Rajapakse, "An Exact Stiffness Method for Elastodynamics of a Layered Orthotropic Half-Plane," *Journal of Applied Mechanics,* vol. 61, no. 2, pp. 339-348, 1994.
[34] R. Piessens, "Quadpack : a subroutine package for automatic integration," ed. Berlin: Springer-Verlag, 1983.
[35] A. Katebi and A. P. S. Selvadurai, "Undrained behaviour of a non-homogeneous elastic medium: The influence of variations in the elastic shear modulus with depth," *Geotechnique,* vol. 63, pp. 1159-1169, 2013.

[36] M. A. Meyers and K. K. Chawla, *Mechanical Behavior of Materials*, 2 ed. Cambridge: Cambridge University Press, 2008.

[37] T. Nakayama, K. Yamamoto, H. Satoh, T. J. Konno, B. M. Clemens, and R. Sinclair, "Structure and corrosion properties of Al/Si and Fe/Zr multilayers," *Materials Science and Engineering: A,* vol. 198, no. 1, pp. 19-24, 1995.

[38] I. N. Sneddon, "The relation between load and penetration in the axisymmetric boussinesq problem for a punch of arbitrary profile," *International Journal of Engineering Science,* vol. 3, no. 1, pp. 47-57, 1965.

[39] M. F. Doerner and W. D. Nix, "A method for interpreting the data from depth-sensing indentation instruments," *J. Mater. Res.,* vol. 1, pp. 601-616, 1986.

APPENDIX

VITA

The author of this thesis, Mr. Kanin Tarntira, was born in Bangkok, Thailand, on February 25, 1994. He obtained his bachelor's degree from Faculty of Engineering, Chulalongkorn University in 2016. After graduation, he decided to continue on his master's degree in civil engineering at Chulalongkorn University in 2016, the same year, under the supervision of Professor Dr. Teerapong Senjuntichai with the financial support from the department of Civil Engineering on the Civil Engineering 100-year Chula scholarship.